

THEORY OF PHOTOSPHERIC EMISSION FROM RELATIVISTIC OUTFLOWS

R. RUFFINI, I. A. SIUTSOU AND G. V. VERESHCHAGIN

ICRANet, 65122, p.le della Repubblica, 10, Pescara, Italy and
ICRA and Dipartimento di Fisica, Università di Roma “Sapienza”, 00185, p.le A. Moro 5, Rome, Italy
Draft version April 15, 2019

ABSTRACT

Relativistic outflows have been studied in the literature with application to such phenomena as microquasars, Active Galactic Nuclei and Gamma Ray Bursts (GRBs). In the latter case the outflow is initially optically thick and its bulk motion is thought to be ultrarelativistic. Two popular models of optically thick outflows exist: the relativistic wind which is assumed to originate from gradual energy release in a compact region of space, and the relativistic shell which is produced by an explosion. In both cases formulas for the optical depth and the corresponding photospheric radius exist in the literature.

In this paper we reexamine the optical depth of ultrarelativistic spherically symmetric outflows and reevaluate the photospheric radius for each model during both the acceleration and coasting phases. The optical depth is computed analytically and its various asymptotic limits are derived. It is shown that for both the wind and the shell models there are two asymptotic solutions for the optical depth during the coasting phase of the outflow. In particular we show that quite counterintuitively a geometrically thin shell may appear as a thick wind for photons propagating inside it. This is a direct consequence of the ultrarelativistic motion of the outflow. For this reason we introduce notions of photon thick and photon thin outflows, which appear more general and better physically motivated with respect to winds and shells.

Photosphere of relativistic outflow is a dynamic surface. We study its geometry and find that the photosphere of photon thin outflow has always a convex shape, while in the photon thick one it is initially convex (there is always a photon thin layer in any outflow) and then it becomes concave asymptotically approaching the photosphere of an infinitely long wind. Then, assuming that photons are emitted with comoving thermal spectrum at the moment when the optical depth decreases to unity (which means that the last scattering surface of photons is well defined), we compute the observed flux and instantaneous spectra for both photon thick and photon thin outflows. We find that both instantaneous and time integrated observed spectra are very close to the thermal one for photon thick outflows, in line with existing studies. It is our main finding that the photospheric emission from the photon thin outflow produces *non thermal* time integrated spectra, which may be described by the Band function well known in the GRB literature.

Our results are then applied to GRBs. We find that energetic GRBs should produce photon thin outflows with photospheric emission lasting less than one second for the total energy $E_0 \leq 10^{54}$ erg and baryonic loading parameter $B \leq 10^{-2}$, independently of the size of energy release region. It means that only time integrated spectra may be observed from such GRBs. In other words, observed Band spectrum is obtained quite naturally from the comoving thermal one by the integration over the photosphere. We stress that this is a purely geometric effect and it comes from an appropriate dependence of temperature and emitting surface on arrival time.

Subject headings: Gamma-ray burst: general – Relativistic processes

1. INTRODUCTION

High Lorentz factors of the bulk motion of various outflows are common in relativistic astrophysics. The best known examples are Active Galactic Nuclei (Maraschi 2003), microquasars and Gamma-Ray Bursts (GRBs) (Piran 2004). In the latter case outflows indeed reach ultrarelativistic velocities. For this reason GRB emission a) originates far from the source of energy release and b) is observed as a transient event with a typical duration on the order of seconds.

Various models are suggested to explain the acceleration of outflows to ultrarelativistic velocities. The electromagnetic model (Lyutikov 2006) assumes that the energy in the source of GRB is converted into electromagnetic energy which is transported in the form of a Poynting flux. We adopt here another popular idea that the energy release leads to creation of an optically thick source which expands due to thermal ac-

celeration. This idea is the basis of both the fireball (Piran 1999) and the fireshell (Ruffini et al. 2009) models.

In pioneer works by Goodman (1986) who considered an instant explosion, and by Paczynski (1986) who discussed a gradual energy release, a conclusion was reached that the electron-positron plasma is created in the source of GRB. Assuming further that the plasma reaches thermal equilibrium they focused on hydrodynamic expansion in such models and gave photometric and spectroscopic predictions for GRBs. Later, baryonic loading of fireballs was considered for explosions by Shemi & Piran (1990) and for winds by Paczynski (1990). Abramowicz et al. (1991) considered the appearance of the photosphere of the relativistic wind to a distant observer showing that it is concave.

The interest to photospheric emission from relativistic winds has been revived recently in papers by Daigne & Mochkovitch (2002), Pe’er et al. (2007), Beloborodov (2011), Ryde et al. (2011), Pe’er & Ryde (2011), and others.

In the fireshell model, which assumes an explosive energy

release, the first potentially visible component of any GRB, the Proper GRB (Bianco et al. 2001), comes from the thermal flash of photons emitted when the outflow becomes transparent for photons.

In this paper we readdress the issue of the photospheres of relativistic outflows using a simple model valid for both instant and gradual energy release. We rederive analytic expression for the optical depth, give asymptotic solutions for the photospheric radius providing clear physical interpretation of our results. Then we present the analytic treatment and fitting formulae for observed flux of photospheric emission assuming isotropic thermal distribution of photons in the comoving frame. Finally, we compute both instantaneous and time-integrated spectra of photospheric emission. These results are then applied within both the shell and the wind models of GRBs.

The structure of the paper is as follows. In Section 2 we discuss, compare and contrast an impulsive explosion and gradual energy release, giving rise respectively to an ultrarelativistic shell and wind. In Section 3 we compute the optical depth and the radius of photosphere of a portion of relativistic wind. Section 4 discusses the geometry and dynamics of the photosphere in the relativistic outflow. In Section 5 we treat the observed flux emerging from the photosphere. Observed spectra are computed in Section 6. Then we apply these results to GRBs in Section 7. Conclusions follow. The case of optical depth along the line of sight of an ultrarelativistic shell with finite thickness is treated in the Appendix A. In Appendix B we consider the high-energy part of the time-integrated spectrum of photon thin outflow with arbitrary density profile.

2. OPTICALLY THICK RELATIVISTIC OUTFLOWS: WIND VS. EXPLOSION

Relativistic outflows are generally classified as winds or shells depending on how fast the energy in their sources is released. Consider energy release in a source of linear dimension R_0 . If the time scale of energy release is short $\Delta t \ll R_0/c$, an explosion occurs, which may be characterized by the size R_0 , total energy released E_0 and total baryonic mass M . When the energy is released gradually, on a time scale $\Delta t \gg R_0/c$, but the source luminosity L exceeds the Eddington limit, a wind is formed, which is characterized by its activity time Δt , luminosity L and mass ejection rate \dot{M} .

It is possible that the temperature in the source of the relativistic outflow is large enough for electron-positron pair creation. In that case e^+e^- pairs make an additional contribution to the optical depth. Whether the outflow becomes relativistic or not depends on the entropy in the region where the energy is released. Both the wind and explosion cases can be parametrized (Ruffini et al. 2000) by a dimensionless baryonic loading parameter

$$B \simeq \begin{cases} \frac{Mc^2}{E_0}, & \text{explosion,} \\ \frac{\dot{M}c^2}{L}, & \text{wind.} \end{cases} \quad (1)$$

When the baryonic loading is sufficiently small the baryons will be accelerated to a relativistic velocity v of bulk motion, attaining large Lorentz factors $\Gamma = [1 - (v/c)^2]^{-1/2}$, while in the opposite case of large baryonic loading the outflow re-

mains nonrelativistic:

$$\Gamma = \Gamma_m \simeq B^{-1}, \quad B \ll 1 \quad (2)$$

$$v \simeq c\sqrt{B/2}, \quad B \gg 1. \quad (3)$$

In what follows we consider only ultrarelativistic spherically symmetric outflows with $\Gamma \gg 1$. In the simplest cases of wind or explosion in vacuum, the dynamics of the outflow is divided into an acceleration phase and a coasting phase (Piran 1999) with respectively

$$\Gamma \simeq \frac{R}{R_0}, \quad n \simeq n_0 \left(\frac{R}{R_0} \right)^{-3}, \quad R_0 < R < \frac{R_0}{B}, \quad (4)$$

$$\Gamma \simeq B^{-1} = \text{const}, \quad n \simeq n_0 \left(\frac{R}{R_0} \right)^{-2}, \quad \frac{R_0}{B} < R < R_{tr}, \quad (5)$$

where R_{tr} is the radius at which the outflow becomes transparent to Thomson scattering and n is the comoving number density of baryons in the outflow. The outflow may also become transparent for photons at the acceleration phase, provided that $R_{tr} < B^{-1}R_0$. Notice that in the case of an impulsive explosion for $r \gg R_0$ the matter and energy appear to a distant observer to be concentrated in a *geometrically thin* shell having width $l \sim R_0$ due to the relativistic contraction.

It is important to stress that both *an infinitely long wind* with a time-independent mass ejection rate and luminosity on the one hand, and *an infinitely thin shell* originating from an instantaneous explosion in infinitely thin region represent two limiting cases for the energy release.

During both acceleration and coasting phases the continuity equation for the laboratory number density reduces to $n\Gamma \propto r^{-2}$. We parametrize generic density profile as

$$n\Gamma = \begin{cases} n_0 \left(\frac{R_0}{r} \right)^2 f(\xi), & R_o(t) - l < r < R_o(t), \\ 0, & \text{otherwise,} \end{cases} \quad (6)$$

where $R_o(t)$ is the equation of motion of the outer boundary of the outflow, $f(\xi)$ is an arbitrary function of the depth ξ of the outflow measured from the outer boundary. Analogously one may introduce the corresponding functions for temperature and Lorentz factor dependences within expanding outflows.

In this paper we focus on a simplest case with constant number density, temperature and Lorentz factor measured by an observer with fixed laboratory radius. This profile corresponds to a portion of relativistic wind with $f(\xi) = 1$. Such an outflow may be produced by a gradual energy release with constant luminosity and mass ejection rate on a finite time Δt and we will refer to it as the *wind*. In Appendix A we consider another density profile, which at certain instant of time measured by a laboratory observer (e.g., at the beginning of the coasting phase) is a constant. It may be interpreted as the average density of the outflow at fixed laboratory time. Such ultrarelativistically expanding outflow with finite thickness l may result from an explosion and we will refer to it as the *shell*. The evolution of the laboratory number density (in the observer's frame) of both wind and shell is shown in Fig. 1. In Appendix B we consider a power law density profile $f(\xi)$. Fig. 1 shows that unlike other profiles only a portion of wind keeps its shape for constant laboratory time.

Below we show that both the shell and the wind defined above may appear for photons emitted inside it as long wind

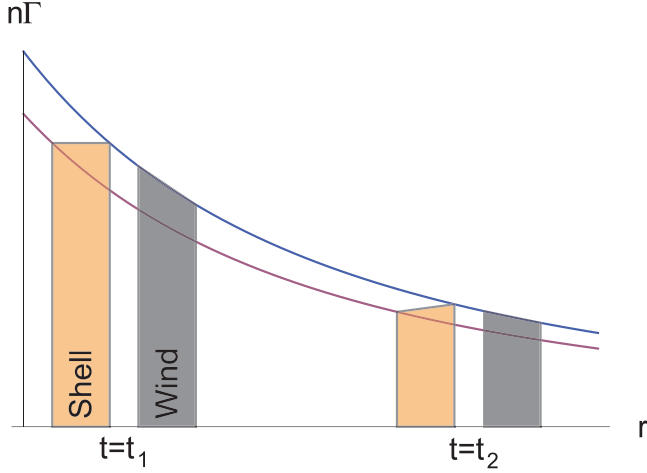


FIG. 1.— The laboratory number density is shown for a shell with initially constant density and a wind with finite duration at two different times $t = t_1$ and $t = t_2$. While the wind preserves the r^{-2} shape, the shape of the shell changes making its density profile steeper with time.

or as thin shell, depending on the initial conditions that specify respectively their width l and activity duration Δt . It is crucial to keep in mind that photons emitted inside the expanding outflow propagate in a medium whose laboratory number density depends both on the radial coordinate and on time $\Gamma(r, t)n(r, t)$. For photons propagating in the wind the spatial dependence of the number density plays the key role, while for photons propagating in the shell its time dependence is crucial.

In the next section we compute the optical depth of the portion of wind. The computation in the case of the shell is provided in Appendix A which shows that the difference between the shell and the wind may be neglected in the ultrarelativistic approximation.

3. OPTICAL DEPTH ALONG THE LINE OF SIGHT

In this section we compute the optical depth of relativistic outflows and determine the corresponding photospheric radii along the line of sight. The optical depth along the photon world line \mathcal{L} is

$$\tau = \int_{\mathcal{L}} \sigma j_{\mu} dx^{\mu}, \quad (7)$$

where σ is the cross section, j^{μ} is the 4-current of particles, on which the photon scatters, and dx^{μ} is the element of the photon world line.

Consider a spherically symmetric expanding outflow with an ultrarelativistic velocity $v = \beta c \simeq 1 - 1/2\Gamma^2$. Assume that the photon is emitted at the interior boundary $r = R$ of the outflow. This assumption is relaxed in the Appendix A. The optical depth computed along the photon path from (7) is (see e.g. Abramowicz et al. (1991))

$$\tau = \int_R^{R+\Delta R} \sigma n \Gamma (1 - \beta \cos \theta) \frac{dr}{\cos \theta}, \quad (8)$$

where $R + \Delta R$ is the radial coordinate at which the photon leaves the outflow, and θ is the angle between the velocity vector of the outflow and the direction of propagation of the photon, n is the comoving number density of electrons and positrons, which may be present due to pair production.

Along the line of sight (8) reduces to

$$\tau = \int_R^{R+\Delta R} \sigma n(R) \Gamma (1 - \beta) dr \approx \int_R^{R+\Delta R} \sigma \frac{n}{2\Gamma} dr. \quad (9)$$

In the remaining part of this section we will consider the optical depth under different conditions characterizing the outflow and derive expressions for the photospheric radius along the line of sight.

3.1. Pure electron-positron plasma

A pure electron-positron plasma reaches thermal equilibrium before expansion and remains thermal and accelerating until it becomes transparent to radiation (Aksenov et al. 2007, 2009, 2010). Comoving number density of electrons and positrons is a function of their comoving temperature, which is decreasing during accelerating adiabatic expansion (e.g. Shemi & Piran (1990)) as

$$T(R) = T_0 \frac{R_0}{R}, \quad (10)$$

where T_0 is the temperature of plasma in the source. Since the transparency temperature is nonrelativistic, $T_{tr} \ll m_e c^2/k$, we can treat electron-positron pairs as nondegenerate and nonrelativistic. Their number density is then

$$n(T) = \frac{1}{\sqrt{2}} \left(\frac{kT m_e}{\pi \hbar^2} \right)^{3/2} \exp\left(-\frac{m_e c^2}{kT}\right). \quad (11)$$

From (9), (10), and (11) we obtain the optical depth along the line of sight

$$\tau = \int_R^{R+\Delta R} \frac{\sigma}{\sqrt{2}} \left(\frac{kT_0 m_e}{\pi \hbar^2} \right)^{3/2} \left(\frac{R_0}{r} \right)^{5/2} \exp\left(-\frac{m_e c^2 r}{kT_0 R_0}\right) dr. \quad (12)$$

Initial temperature T_0 can be expressed in terms of initial size and energy. Then by equating (12) to unity we obtain the radius at which the outflow becomes completely transparent along the line of sight, *the transparency radius* R_{tr} .

Due to exponential dependence on the radial coordinate in (12), transparency is reached at

$$kT_{\pm} \simeq 0.040 m_e c^2 \quad (13)$$

independent of the initial conditions. Note that the optical depth for an expanding electron-positron-photon shell computed by Shemi & Piran (1990) is incorrect since it uses photon thin asymptotics, see (29) below, which never applies to the pure e^+e^- outflows. The formula (13) is in agreement with works of Grimsrud & Wasserman (1998) and Li & Sari (2008).

In the case of the shell with $l \simeq R_0$

$$R_{tr} = \frac{1}{T_{\pm}} \left(\frac{3E_0 l}{4\pi a} \right)^{1/4}, \quad (14)$$

where $a = 4\sigma_{SB}/c$ and σ_{SB} is the Stefan-Boltzmann constant. Analogously in the case of the wind

$$R_{tr} = \frac{1}{T_{\pm}} \left(\frac{E_0 R_0^2}{4\pi l a} \right)^{1/4} = \frac{1}{T_{\pm}} \left(\frac{L R_0^2}{16\pi \sigma_{SB}} \right)^{1/4}, \quad (15)$$

where we used a relation

$$E_0 = L \Delta t \simeq L l / c. \quad (16)$$

3.2. Acceleration phase

Now we focus on the acceleration phase described by (4), assuming that the optical depth (8) along the line of sight corresponds to electrons with density equal to the baryon density n . Here and below we take for the laboratory density a profile (6) with $f(\xi) = 1$ which gives

$$n\Gamma = \begin{cases} n_0 \left(\frac{R_0}{r}\right)^2, & R_o(t) - l < r < R_o(t), \\ 0, & \text{otherwise.} \end{cases} \quad (17)$$

Actually positrons give a contribution to the optical depth even as comoving temperature decreases below (13) due to their freeze out. Their contribution evaluates to

$$\frac{n_{\pm}}{n} = \frac{4\pi l r_{\pm}^2 n_{\pm} \Gamma_{\pm}}{N}, \quad (18)$$

where quantities with subscript \pm refer to the temperature (13), and total number of baryons is obtained from (17) as

$$N = 4\pi n_0 R_0^2 l. \quad (19)$$

In what follows we neglect the electron-positron pair contribution, assuming $n_{\pm} \ll n$.

Assuming that the cross section is constant, and using (4), (9) and (17) one has

$$\begin{aligned} \tau &= \int_R^{R+\Delta R} \sigma n_0 \left(\frac{R_0}{r}\right)^2 \left(\frac{R_0^2}{2r^2}\right) dr = \\ &= \frac{1}{6} \sigma n_0 R_0^4 \left(\frac{1}{R^3} - \frac{1}{(R+\Delta R)^3}\right). \end{aligned} \quad (20)$$

In the ultrarelativistic approximation from equations of motion of the photon and of the outflow one can see that such photon cannot leave the outflow during acceleration phase. Therefore (20) reduces to

$$\tau = \frac{\sigma n_0 R_0^4}{6R^3} = \frac{\sigma N R_0^2}{24\pi R^3 l}. \quad (21)$$

We then obtain the following expression for the transparency radius of the accelerating outflow:

$$R_{tr} = \left(\frac{\sigma N R_0^2}{24\pi l}\right)^{1/3}. \quad (22)$$

Finally we can express the number of baryons in the outflow for either the shell or wind, assuming baryons are represented by protons with mass m_p . For the wind $N = \dot{M}\Delta t/m_p \simeq \dot{M}l/(m_p c)$, where the outflow width is given by $l \simeq c\Delta t$, while for the shell with $l \simeq R_0$ the number of baryons is $N = M/m_p$. Then using (1) we have

$$N = \begin{cases} \frac{E_0 B}{m_p c^2}, & \text{shell,} \\ \frac{L B l}{m_p c^3}, & \text{wind.} \end{cases} \quad (23)$$

As result we obtain for the shell

$$R_{tr} = \left(\frac{\sigma E_0 B R_0^2}{24\pi m_p c^2 l}\right)^{1/3}, \quad (24)$$

and for the wind

$$R_{tr} = \left(\frac{\sigma L B R_0^2}{24\pi m_p c^3}\right)^{1/3}. \quad (25)$$

3.3. Coasting phase

At the coasting phase described by (5), the equation of motion for the external boundary of the outflow is

$$R_o(t) = R + l + c\beta t, \quad (26)$$

so the photon ‘‘sees’’ the expanding outflow $2\Gamma^2$ times thicker than its width measured in the laboratory frame

$$\Delta R = \frac{l}{1-\beta} \simeq 2\Gamma^2 l. \quad (27)$$

The optical depth along the line of sight computed along the path of the photon is again given by (9)

$$\tau = \int_R^{R+\Delta R} \frac{\sigma n_0}{2\Gamma^2} \left(\frac{R_0}{r}\right)^2 dr = \frac{\sigma n_0 R_0^2}{2\Gamma^2} \left[\frac{1}{R} - \frac{1}{R+2\Gamma^2 l}\right]. \quad (28)$$

This expression has two asymptotics, which using (19) can be written as follows

$$\tau = \begin{cases} \frac{\sigma n_0 R_0^2}{2\Gamma^2 R} = \frac{\sigma N}{8\pi\Gamma^2 l R}, & 2\Gamma^2 l \gg R, \\ \frac{\sigma n_0 R_0^2 l}{R^2} = \frac{\sigma N}{4\pi R^2}, & 2\Gamma^2 l \ll R. \end{cases} \quad (29)$$

Finally the transparency radius for the shell is

$$R_{tr} = \begin{cases} \left(\frac{\sigma E_0 B^3}{8\pi m_p c^2 l}\right)^{1/3}, & 2\Gamma^2 l \gg R_{tr}, \\ \left(\frac{\sigma E_0 B}{4\pi m_p c^2}\right)^{1/2}, & 2\Gamma^2 l \ll R_{tr}, \end{cases} \quad (30)$$

while for the wind it is

$$R_{tr} = \begin{cases} \left(\frac{\sigma L B^3}{8\pi m_p c^3}\right)^{1/3}, & 2\Gamma^2 c\Delta t \gg R_{tr}, \\ \left(\frac{\sigma L B \Delta t}{4\pi m_p c^2}\right)^{1/2}, & 2\Gamma^2 c\Delta t \ll R_{tr}. \end{cases} \quad (31)$$

3.4. Discussion

Let us interpret the results obtained above. On the one hand, Eq. (21) and the first line of (29) with $\tau \propto R^{-3}$ and $\tau \propto R^{-1}$ correspond to the case when a photon emitted inside the outflow stays there for a significant time so that it feels its density decreasing with time (or radius). In this respect the photon ‘‘sees’’ the outflow as a long wind, even if the laboratory thickness of the outflow is small, $l \ll R$. We refer to this case as a *photon thick outflow*. On the other hand, the second line in (29) with $\tau \propto R^{-2}$ corresponds to the case when the photon spends too little time inside the outflow to feel its density decreasing with radius (for the wind) or time (for the shell). The photon ‘‘sees’’ the outflow as a thin shell even if the duration of explosion could be long and a wind was launched. We refer to this case as a *photon thin outflow*. In other words, a geometrically thin ultrarelativistically expanding shell may be both thin or thick as viewed by the photon propagating inside it.

Similar consideration may be applied to a photon emitted from any distance ξ from the outer boundary of the outflow (see Appendix A). It is clear then, that even in a photon thick outflow there is always a photon thin layer located near the outer boundary. During acceleration phase such a photon thin part accounts for a fraction not larger than B of the entire width of the outflow.

In the derivation of (29) we used the approximation (17) representing a portion of a relativistic wind. The derivation of the formula for the optical depth with a density profile which at some instant of time preceding photon emission is independent of the radial coordinate is given in the Appendix A. The results for both density profiles are equal, provided that $R \gg l$.

The expressions for the radius of the photosphere of a relativistic wind were obtained in e.g. Mészáros & Rees (2000). These formulas coincide up to a numerical factor (which comes from the integration over the radial coordinate) with our (25) and (31). It should be noted, however, that only the photon thick asymptotic limit is applied in Mészáros & Rees (2000).

The photon thin asymptotic limit may also be valid for relativistic winds in the coasting phase, provided that $l \ll R/(2\Gamma^2)$. This is an independent condition from $\Delta t \gg R_0/c$ and it is therefore possible to give the following constraints for Δt under which the outflow takes the form of a wind, but it is photon thin:

$$\frac{R_0}{c} \ll \Delta t \ll \frac{\sigma LB^5}{16\pi m_p c^4}. \quad (32)$$

Transparency radius for photon thick and photon thin asymptotics for a portion of the coasting relativistic wind (31) was obtained by Daigne & Mochkovitch (2002).

Similar considerations apply to an ultrarelativistic shell which is considered e.g. in Shemi & Piran (1990) and Mészáros et al. (1993) and by Ruffini et al. (2000) in the photon thin approximation. The corresponding condition that the shell appears to be photon thin is

$$c\Delta t \ll R_0 \ll \left(\frac{\sigma E_0 B^5}{16\pi m_p c^2} \right)^{\frac{1}{2}}.$$

It is possible, however, that initial conditions satisfy the opposite constraint

$$R_0 \gg c\Delta t, \quad R_0 \gg \left(\frac{\sigma E_0 B^5}{16\pi m_p c^3} \right)^{\frac{1}{2}},$$

which results in a photon thick shell. This photon thick asymptotic limit has been used by Nakar et al. (2005) following Grimsrud & Wasserman (1998) without any discussion of its applicability. All cases discussed above have been considered by Mészáros et al. (2002), except the transparency of pure electron-positron outflow. Finally, Toma et al. (2011) consider all asymptotic solutions, applying them to a relativistic wind.

Numerical hydrodynamic simulations produce complex density, temperature and Lorentz factor profiles of the outflow. In particular, Piran et al. (1993) and Mészáros et al. (1993) considered an explosion in a compact region with radius R_0 and studied numerically the hydrodynamic evolution of an optically thick plasma with various initial conditions. They have shown that the plasma forms a relativistically expanding shell with some density and velocity profiles. The

characteristic width of the density profile appears to be constant up to large radii, but later it increases linearly with radius due to the fact that the Lorentz factor appears to be monotonically increasing within the shell

$$l \simeq R_0, \quad R < B^{-2}R_0, \quad (33)$$

$$l \propto R, \quad R > B^{-2}R_0. \quad (34)$$

Such a spreading in density profile may result in a substantial increase in the width $l \gg R_0$ of the shell when it becomes transparent to radiation. Note that condition (34) coincides with the condition in the second line of (29), which corresponds to the case of a photon thin outflow. Numerical integration of (9) shows nevertheless that the photon thin asymptotics (29) is valid even for the shell undergoing such spreading.

4. GEOMETRY AND DYNAMICS OF THE PHOTOSPHERE

Unlike traditional static sources usually dealt with in astrophysics, relativistic outflows have strongly time-varying photospheres. For a given laboratory time t the photosphere geometry $r = r(\mu)$ is obtained by equating (8) to unity.

For the portion of wind (17) the optical depth can be calculated analytically both at acceleration and coasting phases for photon thin and photon thick outflows:

$$\begin{aligned} \tau(r, \theta, t) = & \sigma n_0 R_0^2 \left\{ \frac{1}{r \sin \theta} \left[\theta - \tan^{-1} \left(\frac{r \sin \theta}{cT + r \cos \theta} \right) \right] \right. \\ & - \left(1 - \frac{1}{2\Gamma_m^2} \right) \left(\frac{1}{r} - \frac{1}{\sqrt{(cT + r \cos \theta)^2 + (r \sin \theta)^2}} \right) \\ & \left. + \frac{R_0^2}{6} \left(\frac{1}{r^3} - \frac{1}{[(cT + r \cos \theta)^2 + (r \sin \theta)^2]^{3/2}} \right) \right\}, \quad (35) \end{aligned}$$

where T is the time interval during which photon remains inside the outflow, determined by the equations of motion of the photon and of the outflow, and Γ_m is defined by (2).

For the infinitely long relativistic wind with $\beta = \text{const}$ (Abramowicz et al. 1991) $\Delta t, T \rightarrow \infty$, the photosphere is a static surface

$$r = \sigma n_0 R_0^2 \left(\frac{\theta}{\sin \theta} - \beta \right), \quad (36)$$

which has a concave shape for $\beta > 2/3$, see Fig. 2. It appears for a distant observer as a static spot with radius

$$R_{obs} = \pi \sigma n_0 R_0^2 \quad (37)$$

and brightness decreasing from the center to the edge. For the accelerating infinite wind the photosphere is also a static surface and its curvature is larger than that of the coasting wind (see Fig. 2). These static photospheres represent asymptotic limits of the dynamic photospheres of coasting and accelerating photon thick outflows, respectively.

Inside the relativistic beaming cone $\theta = \arccos \beta$ the photosphere of an infinitely thin shell at a fixed laboratory time is an infinitely thin ring. The collection of such rings for all laboratory times represents a surface

$$r = \left(\sigma \Sigma \frac{1 - \beta \cos \theta}{|\cos \theta - \beta|} \right)^{1/2}, \quad (38)$$

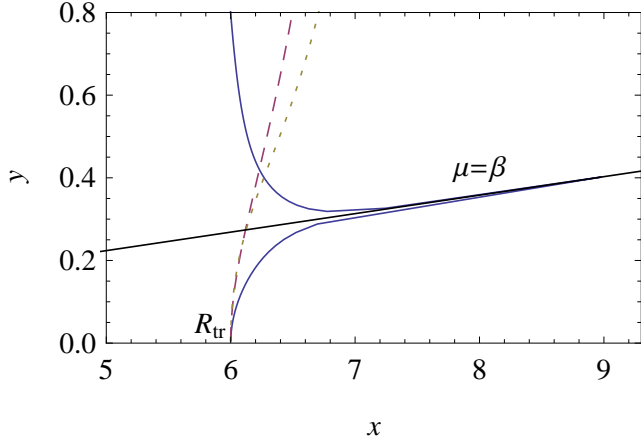


FIG. 2.— The shape of photospheres of infinitely long coasting (dashed curve) and accelerating (dotted curve) winds as well as time-integrated photosphere of infinitely thin shell (solid curve) in logarithmic coordinates $x = \cos \theta \times \log_{10} r_{tr}$, $y = \sin \theta \times \log_{10} r_{tr}$ for $\beta = 1 - 10^{-3}$.

where $\Sigma = n_0 R_0^2 l$ is the shell surface density. The curvature of this surface is even larger than that of accelerating wind, as can be seen from Fig. 2 and the small angle $\theta \ll 1/\Gamma$ expansion of (35)

$$\tau = \begin{cases} \frac{\sigma N l}{24\pi R^3} \left(1 + \frac{R^2 \theta^2}{l^2}\right), & R \ll \Gamma R_0, \\ \frac{\sigma N}{8\pi l \Gamma^2} \left(1 + \frac{1}{3} \Gamma^2 \theta^2\right), & \Gamma R_0 \ll R \ll 2\Gamma^2 l, \\ \frac{\sigma N}{4\pi R^2} (1 + 2\Gamma^2 \theta^2), & R \gg 2\Gamma^2 l. \end{cases} \quad (39)$$

The surface (38) represents asymptotic limit of photospheres of photon thin outflows.

In ultrarelativistic case the surfaces (36) and (38) give the position of the corresponding photon thick and photon thin outflow photospheres with very good accuracy.

The part of dynamic photosphere seen by a distant observer at a given instant of arrival time t_a represents equitemporal surface (EQTS) of the photospheric emission. EQTS has been initially introduced for the GRBs by Bianco et al. (2001). We will refer to that surfaces as *Photospheric EQTS*, (PhE).

4.1. Coasting photon thin case

Geometrical shape of dynamical PhE of the photon thin outflow is similar to EQTS of infinitesimally thin constantly emitting relativistic shell considered firstly by Couderc (1939) and then by Rees (1966, 1967). The EQTS of this shell appears to a distant observer as an ellipsoid with axes ratio equal to Γ . However the PhE of photon thin outflow is not the entire ellipsoid: it is only a part of that surface, see Fig. 6. The external boundary of the surface for a given t_a is defined by the condition $\tau(\xi = 0, \mu, t_a) = 1$, which means that the optical depth of photons emitted from the outermost layer of the outflow equals unity. In the photon thin asymptotics this surface coincides with the relativistic beaming cone $\mu = \beta$. As soon as the outflow reaches the transparency radius given by the second lines of (30) for the shell or (31) for the wind an internal boundary appears as well. The surface of internal boundaries is described by (38), see also Fig. 6.

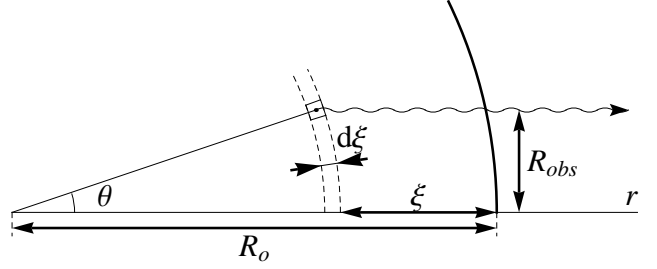


FIG. 3.— Geometry and illustration of variables used for calculation of the flux received from relativistically expanding outflow. Observer is located to the right at infinity.

4.2. Accelerating and coasting photon thick cases

As we already mentioned in Sec. 3.4, in a photon thick outflow there is always an external photon thin layer. Since this layer gets transparent first, initial evolution of PhE in the photon thick case is similar to the photon thin one. When transition to the photon thick asymptotics occurs, initially convex PhE of the photon thin layer of the outflow transforms to a concave PhE of its photon thick part, see Fig. 4 and Fig. 7 for accelerating and coasting cases, respectively. This concave PhE in both cases approaches the photosphere of infinitely long wind. In the coasting case the approach to the surface (36) is only asymptotic, while in the accelerating case the photosphere actually reaches it at finite arrival time. Similarly to the photon thin case, there exists an external boundary of the PhE determined by the same condition, and shown in Fig. 7. Notice that this boundary is wider than the relativistic beaming surface (these are tube and cone for accelerating and coasting outflows, respectively). As soon as the innermost part of the outflow reaches the transparency radius, i.e. observer sees the switching off of the wind, the inner boundary of the PhE appears with increasing $\theta(t_a)$. The surface of these boundaries is given by (36) in the case of coasting photon thick outflow.

5. OBSERVED FLUX

In this section we consider the appearance of the outflow photosphere to a distant observer and describe time evolution of luminosity in adiabatic approximation.

5.1. Adiabatic approximation for evaluation of observed flux

Take a volume element dV located at the laboratory radial distance ξ from the outer boundary of the outflow at angular separation θ from the line of sight, see Fig. 3. It is convenient to introduce the notation $\mu = \cos \theta$. The basic assumption of our method is that photons are locked inside this volume element for $\tau(\xi, \mu, t) > 1$ and stream freely when the optical depth decreases below unity. In this approximation we neglect diffusion of photons from the optically thick outflow. Besides, we assume that all photons at given (ξ, μ) are emitted simultaneously. It means that the last scattering surface defined by the condition $\tau = 1$ is infinitely thin. The probability of photon emission is δ function in (ξ, μ) . Laboratory volume of this element is then

$$dV = 2\pi r(t)^2 d\mu d\xi. \quad (40)$$

Photons are emitted to the observer from the element at the laboratory time $t_e(\xi, \mu)$ defined by

$$\tau(\xi, \mu, t_e) = 1, \quad (41)$$

when the radial coordinate of the element, determined from the equation of motion at given t_e , is $r = R_e(\xi, \mu)$. Emitted energy is obtained from the energy density per unit solid angle $u(\Omega)$ as

$$dE_{obs} = u(\Omega)dVd\Omega = \frac{I}{c}dVd\Omega, \quad (42)$$

where $d\Omega$ is the solid angle of the observer's detector as seen from the photosphere in the laboratory frame and I is bolometric intensity of radiation (see e.g. Eq. (1.6) of Rybicki & Lightman (1979)). Assuming isotropic photon distribution in the comoving frame $I_c = \text{const}$ we get in the laboratory frame (see e.g. Eq. (4.97b) of Rybicki & Lightman (1979))

$$I(\mu) = \frac{I_c}{\Gamma^4(1-\beta\mu)^4} = \Lambda^{-4}I_c, \quad (43)$$

where $\Lambda = \Gamma(1-\beta\mu)$, and finally changing from I_c to the laboratory energy density ε we arrive to (see e.g. Eq. (382) of Pauli (1958))

$$dE_{obs} = \frac{d\Omega}{4\pi} \frac{\varepsilon}{\Gamma^2(1+\beta^2/3)\Lambda^4} dV \simeq \frac{3\varepsilon}{16\pi\Gamma^2\Lambda^4} dVd\Omega. \quad (44)$$

Define the arrival time of that radiation as

$$t_a = t_e - \mu R_e/c, \quad (45)$$

i.e. as time delay with respect to a "trigger" photon emitted at $t_e = 0$, $R_e = 0$ (see e.g. Pe'er & Ryde (2011)). The observed flux at a given t_a is obtained by integration of $dF = \frac{dE_{obs}}{dt_a}$ over the PhE.

5.2. Acceleration phase

When transparency is achieved at acceleration phase (4) the equation of motion of the element dV is

$$r(\xi, t) = \sqrt{R_0^2 + (ct - \xi)^2}, \quad t > \xi/c. \quad (46)$$

Entropy conservation gives for laboratory energy density

$$\varepsilon = \varepsilon_0(R_0/r)^2. \quad (47)$$

Using μ as integration variable over the outflow PhE, the element of observed bolometric flux becomes

$$dF = \frac{dE_{obs}}{d\xi} \frac{\partial \xi}{\partial t_a} = \frac{3}{8} \left(\frac{R_0}{R_e} \right)^6 \frac{\varepsilon_0 R_0^2 d\Omega d\mu}{[1-\beta(R_e)\mu]^4} \frac{\partial \xi}{\partial t_a}, \quad (48)$$

where $\beta(R_e) = \sqrt{1 - R_0^2/R_e^2}$.

The observed flux as function of arrival time is represented in Fig. 4 by thick red curve. The characteristic raising and decaying time is

$$\delta t = R_0^2/(R_{tr}c). \quad (49)$$

There is no simple analytic expression describing the light curve. For large enough $\Delta t \gg \delta t$ the light curve has almost rectangular shape due to the fact that its increase and decay times are much shorter than Δt .

The outflow appears to a distant observer as a spot with size $R_{obs} = \sqrt{R_0^2 - (t_a/c)^2}$, for $-R_0/c \leq t_a \leq 0$. As soon as the PhE reaches the corresponding accelerating infinitely long wind photosphere at $t_a = 0$ the spot size starts to increase almost linearly $R_{obs} \simeq R_0 + ct_a$, see Fig. 4. Finally, as the innermost part of the outflow reaches the transparency radius the spot transforms to a ring with rapidly decreasing width and brightness.

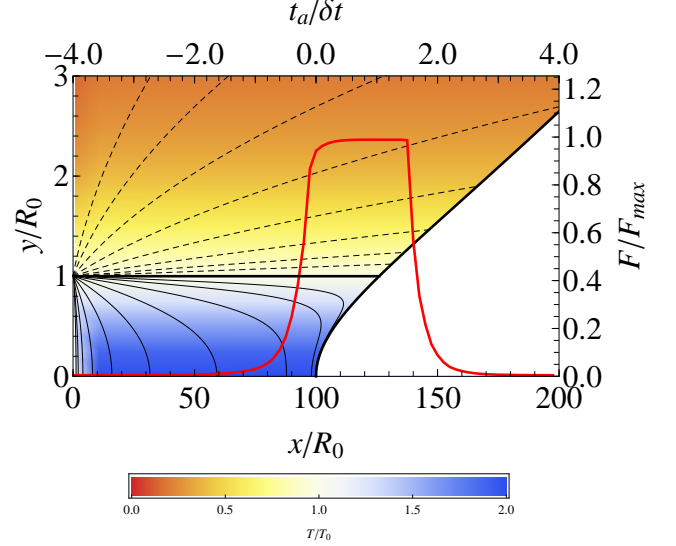


FIG. 4.— Evolution of PhE and the light curve of photospheric emission (red thick curve) from the photon thick accelerating outflow. Thick black curve represents the photosphere of infinitely long accelerating wind. PhEs shown by thin curves correspond from right to left to arrival times $t_a = (-2^{-10}\delta t, -2^{-9}\delta t, \dots)$, see (49). The surface $\mu = \beta$ is given by $R_{obs} = R_0$ and it is shown by thick black line. Dashed curves show the maximal visible R_{obs} for $t_a = (2^{-10}\delta t, 2^{-9}\delta t, \dots)$ from bottom to top. The PhE at that arrival times is a part of the wind photosphere limited by the corresponding curves. Observed temperature of photospheric emission is illustrated by color, see legend. Here $R_{tr} = 100R_0$, and $\Delta t = 2\delta t$.

5.3. Coasting phase

At the coasting phase the element of the outflow has the following equation of motion

$$r(t) = \beta ct - \xi, \quad \mu(t) = \mu = \text{const}. \quad (50)$$

Arrival time of the photospheric emission (45) from that element

$$t_a = \frac{R_e}{\beta c} (1 - \beta\mu) + \frac{\xi}{\beta c} \quad (51)$$

depends on time of emission and μ as

$$t_e = \frac{R_e(\xi, \mu) + \xi}{\beta c}. \quad (52)$$

Entropy conservation at the coasting phase gives (see e.g. Piran et al. (1993))

$$\varepsilon = \varepsilon_0(R_0/r)^{8/3}. \quad (53)$$

Change of variables can be made from μ to t_a and the observed bolometric flux from the element dV is then

$$dF = \frac{dE_{obs}}{d\mu} \frac{\partial \mu}{\partial t_a} = \frac{3}{8} \frac{R_0^{8/3} d\Omega}{c^4 \Gamma^6} \frac{\varepsilon_0 R_e^{10/3} d\xi}{\left(t_a - \frac{\xi}{\beta c} \right)^4 \left| \frac{R_e}{c} - \frac{d \ln R_e}{d\mu} \left(t_a - \frac{\xi}{\beta c} \right) \right|}. \quad (54)$$

The first parenthesis in denominator is the consequence of relativistic beaming, while the second one describes geometry of the photosphere. The observed flux from the outflow is obtained by integration over ξ from 0 to ξ_{max} which is obtained from the position of the PhE at the line of sight, see Fig. 5.

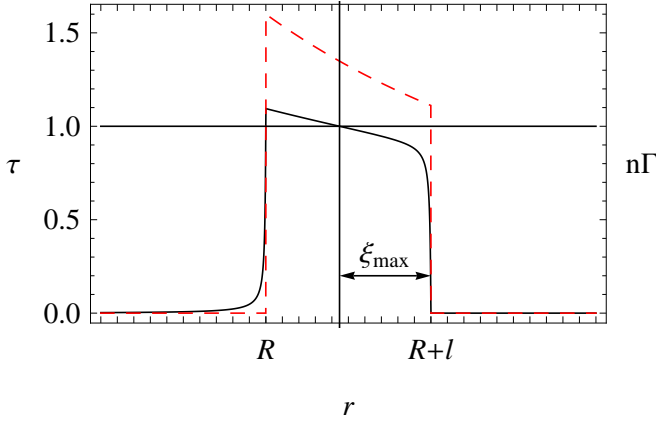


FIG. 5.— Optical depth along the line of sight (black solid line) and laboratory density profile (red dashed line) at the coasting phase for density profile (17) with $\Gamma = 20$ at $t = \text{const.}$

Now we compute the photospheric emission from the coasting photon thin and photon thick outflows. In the case of the portion of wind (17) ξ_{max} can be found analytically:

$$\xi_{\text{max}} = \frac{\beta}{2(1-\beta)} \left\{ [t_a(2-\beta) + D] - \sqrt{[t_a(2-\beta) + D]^2 - 4t_a^2(1-\beta)} \right\}, \quad (55)$$

where

$$D = \sigma n_0 r_0^2 / (2\Gamma^2)^2. \quad (56)$$

The function $R_e(\xi, \mu)$ defined by (41) cannot be found in closed analytic form. Nevertheless the flux can be evaluated numerically and it can be well fitted by the following expression

$$dF \simeq \begin{cases} 0, & t_a < t_0, \\ F_0 \left[1 + \left(\frac{D}{\xi} \right)^{5/6} \right] \left(\frac{t_0 - \frac{\xi}{\beta c}}{t_a - \frac{\xi}{\beta c}} \right)^3 d\xi, & t_a > t_0, \end{cases} \quad (57)$$

where

$$t_0(\xi) = \frac{\xi}{\beta c} \left[1 + \frac{\beta}{2} \left(\sqrt{1 + \frac{4D}{\beta \xi}} - 1 \right) \right] \quad (58)$$

is the minimal arrival time of photons emitted from the outflow at given ξ along the line of sight. This form of pulses is generally referenced in the literature as FRED-like, i.e. fast rise, exponential decay pulses (Fenimore et al. 1996), although decay is not exponential but has a power-law shape. Integration of (57) over ξ gives the form of the light curve of the photospheric emission.

The photon thin outflow initially appears to a distant observer as a bright spot with increasing radius

$$R_{\text{obs}} = \Gamma c t_a \quad (59)$$

and bolometric flux

$$F \propto t_a^{1/3}, \quad (60)$$

see the raising part of the light curve in Fig. 6. The peak flux is reached at

$$t_p \simeq \frac{R_{\text{tr}}}{2\Gamma^2 c}, \quad (61)$$

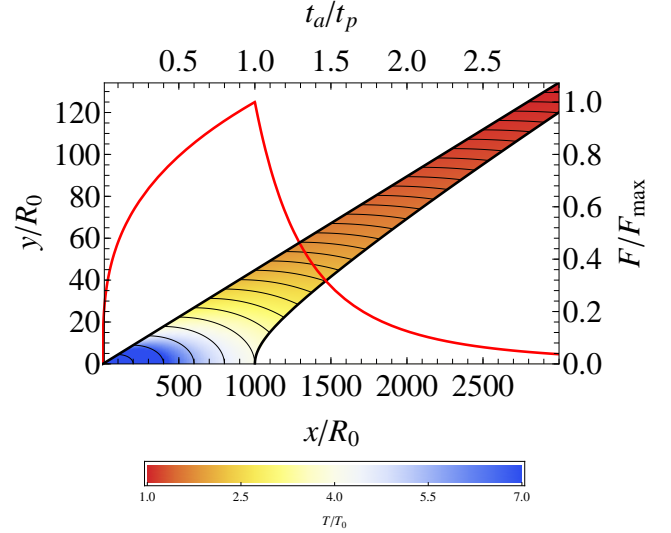


FIG. 6.— Evolution of PhE and the light curve (thick red curve) of photospheric emission from the photon thin coasting outflow. PhEs shown by thin curves correspond from left to right to arrival times $t_a = (t_p/5, 2t_p/5, \dots)$, see (61). Thick black curves bounding PhEs correspond to the position of transparency of the innermost part of the outflow $\xi = l$ (lower curve) and the surface $\mu = \beta$ (upper curve). Observed temperature of photospheric emission is illustrated by color, see legend. Here $\beta = 1 - 10^{-3}$.

when the observer sees photons emitted from the innermost part of the outflow. Then the spot transforms to a ring with steeply decreasing thickness and brightness resulting in the observed flux

$$F \propto t_a^{-3}, \quad (62)$$

see the decaying part of the light curve in Fig. 6.

The observed photospheric emission of the photon thick outflow starts similarly to the previous case, namely a spot with flux increasing as (60), due to the presence of the outer photon thin layer. Then transition to the photon thick asymptotics results in the corresponding change of flux to

$$F = F_{\text{max}} [1 - (t_p/t_a)^2], \quad (63)$$

i.e. increase up to the saturation value $F_{\text{max}} \propto L$, see the raising part of the light curve in Fig. 7. As soon as the arrival time exceeds $t_p + \Delta t$ the flux starts to decrease rapidly

$$F \propto t_p^2 \left[\frac{1}{(t_a - \Delta t)^2} - \frac{1}{t_a^2} \right], \quad (64)$$

and for $t_a \gg \Delta t$ the flux again behaves like (62), see the decreasing part of the light curve in Fig. 7.

The photon thick outflow is observed initially as a spot with radius increasing linearly in t_a as (59), and then reaching its maximal size (37). Again as the innermost part of the outflow approaches the wind photosphere (36) along the line of sight, the spot transforms to a ring, see Fig. 7.

Similarly to the accelerating photon thick outflow the light curve for $\Delta t \gg t_p$ has almost rectangular shape due to the fact that its increase and decay times are much shorter than Δt .

5.4. Discussion

It should be noted that expression (62) is known in the literature for the bolometric flux of instantaneously flashing shell (e.g. Fenimore et al. (1996); Granot et al. (1999a,b);

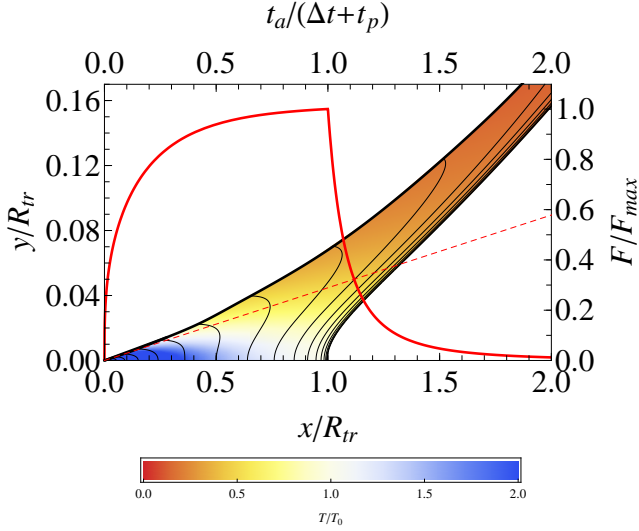


FIG. 7.— Evolution of PhE and the light curve (thick red curve) of photospheric emission of a photon thick coasting outflow. PhEs shown by thin curves correspond from left to right to arrival times $t_a = (10^{-2}t_p, 10^{-1.75}t_p, 10^{-1.5}t_p, \dots)$, see (61). Thick black curves bounding PhEs correspond to the position of infinite wind photosphere (lower curve) and the maximal visible angles at given t_a (upper curve). Notice that these angles exceed the relativistic beaming angle $\mu = \beta$, shown by dashed red line. Observed temperature of photospheric emission is illustrated by color, see legend. Here $\beta = 1 - 10^{-3}$ and $\Delta t = 5t_p$.

Woods & Loeb (1999)). It may be obtained from the expression for detected spectral flux (see Granot et al. (1999b,a))

$$F_\nu(t_a) \propto \int_0^\infty 2\pi r^2 dr \int_{-1}^1 d\mu \Lambda^{-2} j'_{\nu'}(\vec{n}', r, t_a + r\mu/c), \quad (65)$$

where j' is the emissivity of the matter in its comoving frame (the energy per unit time per unit volume per unit frequency per unit solid angle), $\nu' = \Lambda\nu$ is the corresponding frequency of emission, and \vec{n}' is the direction to the detector in that frame. Assuming isotropic emissivity in the comoving frame and integrating over the spectrum one arrives to the bolometric flux

$$F(t_a) \propto \int_0^\infty 2\pi r^2 dr \int_{-1}^1 d\mu \Lambda^{-3} \int_0^\infty j'(\nu', r, t_a + r\mu/c) d\nu', \quad (66)$$

and for instantaneously flashing shell with

$$\int j'(\nu', r, t_a + r\mu/c) d\nu' \propto \delta(r-R) \delta\left(t_a + \frac{r\mu}{c} - \frac{R}{\beta c}\right) \quad (67)$$

expression (62) is recovered.

Actually (65) is incorrect. All the above mentioned works did not account for the transformation in the computation of observed flux from the laboratory time t to the arrival time t_a for dynamic emitter (see, e.g. page 141 of Rybicki & Lightman (1979)). Accounting for that effect we have an additional multiplier $(1 - \beta\mu)^{-1}$ appearing in the integral (65) and correspondingly in Eq. (3) of Granot et al. (1999a), that gives for the bolometric flux after the integration over ν

$$F(t_a) = F_0 t_a^{-4}, \quad \frac{R}{\beta c} (1 - \beta) < t_a < \frac{R}{\beta c} (1 + \beta). \quad (68)$$

The same result can be actually obtained from (57). Analogous mistake was done in the work of Woods & Loeb (1999),

and all the subsequent articles are suffering from the same problem, see e.g. Genet & Granot (2009).

Correct expressions for spectral and bolometric fluxes were obtained by Chiang & Dermer (1999) and by Ruffini et al. (2002). Using transformation laws for intensity of radiation from comoving to laboratory frame (see Equation before (381b) of Pauli (1958)) the expression for spectral flux instead of (65) becomes

$$F_\nu(t_a) \propto \int_0^\infty 2\pi r^2 dr \int_{-1}^1 d\mu \Lambda^{-3} j'_{\nu'}(\vec{n}', r, t_a + r\mu/c). \quad (69)$$

Finally, we discuss the applicability of our adiabatic approximation. Beloborodov (2011) considered the photospheric emission from infinitely long wind both at acceleration and coasting phases and solved the corresponding radiative transfer equation. His main conclusion is that in addition to usual relativistic beaming leading to anisotropy of radiation in laboratory frame (43), in the coasting wind there develops another anisotropy in the comoving frame of the outflow. This comoving anisotropy results from the fraction of photons which already underwent their last scattering in the bulk photon field of the outflow. The anisotropy of such photons grows with increasing radius for geometrical reasons. Since the amount of such photons increases with radius the intensity of the entire photon field becomes increasingly anisotropic. Such phenomenon is referred to as "fuzzy photosphere".

We expect this additional anisotropy in the case of photon thick coasting outflows. In other words, in photon thick outflows the probability distribution of last scattering positions is wide in radius and angles, see also Pe'er (2008). For photon thin outflows instead such effect is not relevant. It is possible to show that practically all photons leave the outflow before the above mentioned anisotropy develops. It means that the corresponding probability distribution is sharp in radius.

In order to describe the late-time photospheric emission of switching off relativistic wind Pe'er (2008) considered emission from a single differential layer. He proposed a model for calculation of observed flux and spectrum based on the probability density function describing the last scattering of photons. Actually he computes not the traditional energy flux understood as energy crossing unit area in unit time, but photon flux as number of photons crossing unit area in unit time. For this reason his decay law for photon flux at late times is

$$F^{ob}(t_a) \propto t_a^{-2}. \quad (70)$$

Lorentz transformation of the photon energy from the comoving frame to the laboratory one results in additional multiplier $(1 - \beta\mu)^{-1}$ in the energy flux that leads to the observed flux $F \propto t_a^{-3}$, which agrees with our (57).

We conclude that adiabatic approximation used in our computation is clearly applicable for photon thin outflows due to the presence of well defined, sharp last scattering surface. As for photon thick outflows our simple adiabatic approximation gives the same results for the bolometric flux as more accurate treatments of radiation transfer (Beloborodov 2011) and of probability density function (Pe'er 2008).

6. INSTANTANEOUS AND TIME-INTEGRATED SPECTRA FROM THE PHOTOSPHERE

In the adiabatic approximation the observed temperature T_{obs} of the PhE depends on angle θ and arrival time t_a :

$$T_{obs}(t_a, R_e(\mu)) = \frac{T_c(R_e(\mu))}{\Gamma(1 - \beta\mu)}, \quad (71)$$

where $T_c(R_e)$ is the comoving temperature on the PhE. When temperature dependence on radius is given, the distribution of observed temperatures across the PhE may be obtained from (71).

Luminosity of photospheric emission is proportional to the volume of the outflow that becomes transparent to radiation at angle θ between t_a and $t_a + dt_a$, i.e. to

$$v_b = \left. \frac{d\xi}{dt_a} \right|_{\mu=\text{const}}, \quad (72)$$

which we will refer to as the *blooming velocity*. Finally, assuming thermal spectrum in the comoving frame the differential spectral flux is

$$dF_\nu = \frac{dE_{\text{obs}}}{d\nu dt_a} = \frac{2h}{c^3} \frac{\nu^3 d\Omega}{\exp\left(\frac{h\nu}{kT_{\text{obs}}}\right) - 1} 2\pi R_e^2 v_b d\mu. \quad (73)$$

Blooming velocity v_b can be obtained from equations of motion of PhE and that of the outflow. In the case of photon thick outflow it is ultrarelativistic and is approximately given by the velocity of the outflow itself since its PhE quickly becomes almost static. From (51) and (53) for transparency at accelerating phase we have

$$T_{\text{obs}}(t_a, \mu) = \left(\frac{R_0}{R_e}\right)^2 \frac{T_0}{1 - \mu \sqrt{1 - \left(\frac{R_0}{R_e}\right)^2}}, \quad (74)$$

while at coasting phase

$$T_{\text{obs}}(t_a, \mu) = \left(\frac{R_0}{R_e}\right)^{2/3} \frac{T_0}{\Gamma(1 - \beta\mu)} = \frac{T_0 R_0^{2/3} R_e^{1/3}}{\Gamma(t_a \beta c - \xi)}. \quad (75)$$

6.1. Photon thin outflow

Instantaneous spectrum of a photon thin outflow integrated over PhE is very close to the thermal one for both accelerating and coasting phases. At accelerating phase observed temperature does not vary with arrival time. At coasting phase observed temperature decreases as

$$T \propto t_a^{-2/3}, \quad (76)$$

while emitting area increases as

$$A \propto t_a^3, \quad (77)$$

leading to the increase of flux (60). For $t_a > t_p$ the emitting area starts to decrease

$$A \propto t_a^{-1/3}, \quad (78)$$

leading to diminishing flux as described by (62).

It can be seen from Fig. 6, that temperature across a given PhE is practically constant. Actually, the radial coordinates of the PhE change only twice between $\theta = 0$ and $\theta = 1/\Gamma$. That is converted by (75) to even smaller temperature interval: from the temperature at the line of sight T_{LOS} to $T_{\text{LOS}}/\sqrt{2}$ at $\theta = 1/\Gamma$.

Integrating these instantaneous spectra over t_a a non thermal spectrum is obtained. It may be represented as Band function (Band et al. 1993) with low-energy power law index $\alpha \simeq 0.5$ and high-energy power law index $\beta = -4$, see Fig. 8. There is an additional cutoff in that spectrum at a very high frequency corresponding to initial temperature of the outflow T_0 .

Evolution of instantaneous spectrum with arrival time depends on assumed outflow density profile (17). Time evolution of observed temperature is determined by entropy conservation so it does not depend on assumed density profile. But emitting area dependence on arrival time actually does depend on it due to change in the blooming velocity, see Appendix B. Low-energy power law index is quite insensitive to the form of both density and temperature profiles. However high-energy part of the time-integrated spectrum of photon thin outflows strongly depends on it. In particular, for power law density profiles (6) with slope δ the high-energy part of the spectrum is

$$F_\nu \propto \nu^{-\frac{3}{1+\delta}}. \quad (79)$$

The resulting β parameter of the Band spectrum may vary from $-\infty$ (exponential cutoff) for $\delta = -1$ to -1 for $\delta = \infty$. For details of high-energy time-integrated spectrum see Appendix B.

6.2. Photon thick outflow

The photospheric spectrum of both accelerating and coasting photon thick outflows evolves through three phases. Initially photon thin layer of the outflow gets transparent, which is described in the previous subsection. Then the PhE becomes concave and it approaches the corresponding static surface, see Figs. 4 and 7 for accelerating and coasting phases respectively. Both accelerating and coasting photon thick outflows exhibit spectra close to thermal ones, see Figs. 9 and 10. The spectra do not evolve until observer detects emission from the innermost part of the outflow, when third phase of spectral evolution begins with very fast decrease of both temperature and emitting area.

Considering time-integrated spectrum we find that as characteristic times of the first and third phases are much less than that of the second one, they do not affect its main part, and the spectrum is close to the thermal one.

6.3. Discussion

Goodman (1986) was the first to obtain the observed spectrum of outflow resulting from instant explosion without any baryonic loading. He found that it is slightly broader than the pure thermal spectrum. Similar conclusion was later reached by Grimsrud & Wasserman (1998) who considered a static

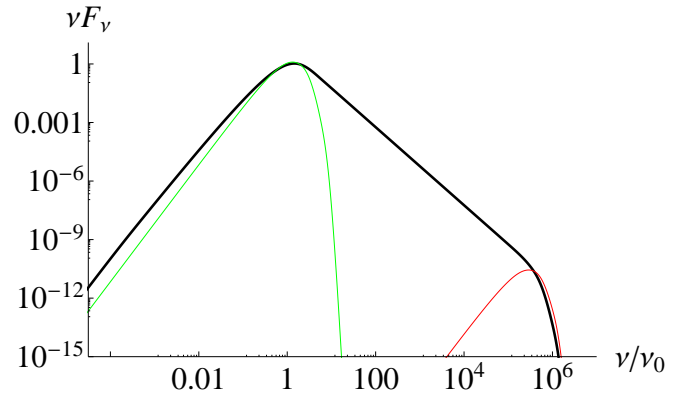


FIG. 8.— Time-integrated spectrum of photospheric emission of photon thin outflow (thick curve, $\Gamma = 100$), superimposed with two instantaneous spectra of that emission, corresponding to arrival time of photons emitted at the moment of transition from acceleration to coasting (thin red curve on the right) and to arrival time of complete LOS transparency of the outflow at $t_a = t_p$ (thin green curve on the left).

wind created by electron-positron pairs. The observed spectrum of photospheric emission from relativistic wind with baryonic loading and variable Lorentz factor was obtained by Daigne & Mochkovitch (2002). Again they found it slightly broader than the thermal one. The results obtained with our adiabatic approximation are in agreement with the above mentioned works.

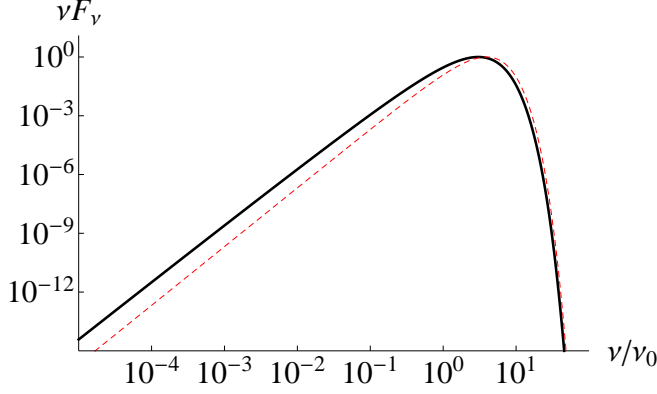


FIG. 9.— Instantaneous spectrum of photospheric emission of accelerating photon thick outflow (thick curve, Lorentz factor at transparency radius $\Gamma = 100$). Dashed red curve represents the thermal spectrum with the temperature T_{LOS} .

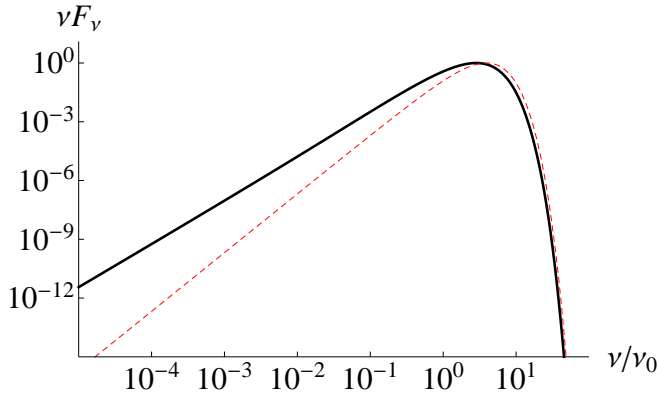


FIG. 10.— Instantaneous spectrum of photospheric emission of coasting photon thick outflow (thick curve, Lorentz factor $\Gamma = 100$). Dashed red curve represents the thermal spectrum with the temperature T_{LOS} .

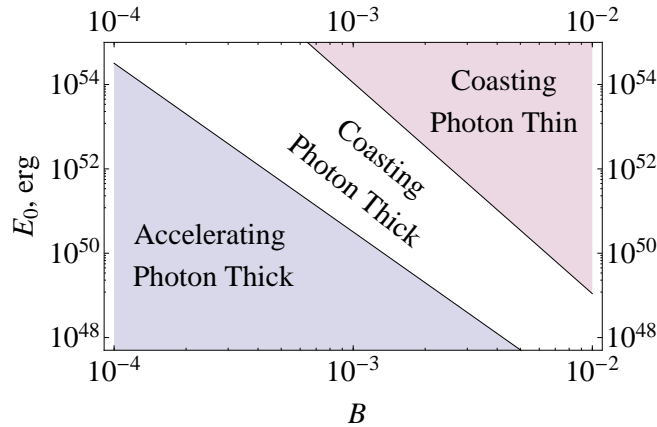


FIG. 11.— The energy-baryonic loading diagram showing the validity of the various asymptotic solutions for the transparency radius for typical parameters of GRBs with $l = R_0 = 10^8$ cm.

Using the probability density function method Pe'er & Ryde (2011) have computed the observed spectrum form switching off relativistic wind. They found that at late times it becomes flat over a wide spectral range. This effect comes from wide distribution of probability of photon last-scattering, the same effect as "fuzzy photosphere" of Beloborodov (2011). Therefore we expect this effect to be present in photon-thick outflows at $t_a > t_p + \Delta t$.

7. APPLICATION TO GRBS

Now we apply the theory of photospheric emission from ultrarelativistic outflows developed in previous sections to GRBs. For simplicity we will neglect cosmological corrections which reduce the observed energy by a factor $(1+z)$ and increase the arrival time by the same factor.

7.1. Shell model

In this subsection we focus on instantaneous explosion producing an ultrarelativistic shell, and apply our results considering typical parameters of GRBs expressing their total energy as $E_0 = 10^{54} E_{54}$ erg, initial size as $R_0 = 10^8 R_8$ cm and baryonic loading parameter as $B = 10^{-2} B_{-2}$.

Summarizing the results obtained above, and taking for σ the Thomson cross section we have for the radius of transparency the following asymptotic solutions together with domains of their applicability

$$R_{tr} = \begin{cases} \frac{1}{T_{tr}} \left(\frac{3E_0 R_0}{4\pi a} \right)^{1/4} = 4.4 \times 10^{10} (E_{54} R_8)^{1/4} \text{ cm}, \\ E_{54} \ll 4.8 \times 10^{-20} B_{-2}^4 R_8^{-1}, \\ \left(\frac{\sigma E_0 B R_0}{24\pi m_p c^2} \right)^{1/3} = 1.8 \times 10^{12} (E_{54} B_{-2} R_8)^{1/3} \text{ cm}, \\ 4.8 \times 10^{-20} B_{-2}^4 R_8^{-1} \ll E_{54} \ll 3.2 \times 10^{-8} B_{-2}^4 R_8^2, \\ \frac{\sigma E_0 B^3}{8\pi m_p c^2 R_0} = 1.8 \times 10^{17} E_{54} B_{-2}^3 R_8^{-1} \text{ cm}, \\ 3.2 \times 10^{-8} B_{-2}^4 R_8^2 \ll E_{54} \ll 1.1 \times 10^{-5} B_{-2}^5 R_8^2, \\ \left(\frac{\sigma E_0 B}{4\pi m_p c^2} \right)^{1/2} = 5.9 \times 10^{14} (E_{54} B_{-2})^{1/2} \text{ cm}, \\ E_{54} \gg 1.1 \times 10^{-5} B_{-2}^5 R_8^2. \end{cases} \quad (80)$$

For very small baryonic loading, or in other words for a pure electron-positron plasma, the transparency radius does not depend on B parameter, then it increases as $B^{1/3}$ (accelerating photon thick solution), then it steeply increases as B^3 (coasting photon thick solution), and finally it increases as $B^{1/2}$ (coasting photon thin solution), see Fig. 12. In Fig. 12 we also show as function of the baryonic loading parameter the following quantities computed at the transparency radius: the Lorentz factor, the observed and comoving LOS temperatures, fraction of energy emitted from the photosphere to

TABLE 1

TABLE OF DEPENDENCIES OF TRANSPARENCY PARAMETERS ON EXPLOSION INITIAL CONDITIONS: ENERGY E_0 , BARYONIC LOADING B , AND RADIUS R_0

Regime of transparency	R_{tr}			Γ_{tr}			kT_{tr}			kT_{obs}		
Pair	$E_0^{1/4}$		$R_0^{1/4}$	$E_0^{1/4}$		$R_0^{-3/4}$	0.040 $m_e c^2$			$E_0^{1/4}$		$R_0^{-3/4}$
Acceleration	$E_0^{1/3}$	$B^{1/3}$	$R_0^{1/3}$	$E_0^{1/3}$	$B^{1/3}$	$R_0^{-2/3}$	$E_0^{-1/12}$	$B^{-1/3}$	$R_0^{-1/12}$	$E_0^{1/4}$		$R_0^{-3/4}$
Coasting photon thick	E_0	B^3	R_0^{-1}		B^{-1}		$E_0^{-5/12}$	$B^{-5/3}$	$R_0^{7/12}$	$E_0^{-5/12}$	$B^{-8/3}$	$R_0^{7/12}$
Coasting photon thin	$E_0^{1/2}$	$B^{1/2}$			B^{-1}		$E_0^{-1/12}$		$R_0^{-1/12}$	$E_0^{-1/12}$	B^{-1}	$R_0^{-1/12}$

TABLE 2

TABLE OF DEPENDENCIES OF TRANSPARENCY PARAMETERS ON WIND INITIAL CONDITIONS: ENERGY RELEASE RATE L , DURATION Δt , AND RADIUS R_0 . DEPENDENCE ON BARYONIC LOADING B IS THE SAME AS IN THE CASE OF SHELL

Regime of transparency	R_{tr}			Γ_{tr}			kT_{tr}			kT_{obs}		
Pair	$L^{1/4}$		$R_0^{1/2}$	$L^{1/4}$		$R_0^{-1/2}$	0.040 $m_e c^2$			$L^{1/4}$		$R_0^{-1/2}$
Acceleration	$L^{1/3}$		$R_0^{2/3}$	$L^{1/3}$		$R_0^{-1/3}$	$L^{-1/12}$		$R_0^{-1/6}$	$L^{1/4}$		$R_0^{-1/2}$
Coasting photon thick	L						$L^{-5/12}$		$R_0^{1/6}$	$L^{-5/12}$		$R_0^{1/6}$
Coasting photon thin	$L^{1/2}$	$\Delta t^{1/2}$					$L^{-1/12}$	$\Delta t^{-1/3}$	$R_0^{1/6}$	$L^{-1/12}$	$\Delta t^{-1/3}$	$R_0^{1/6}$

the total energy, for different values of the total energy E_0 . Dependence of parameters of transparency on initial conditions is also illustrated in Tab. 1. It is clear that the highest Lorentz factors at transparency radius are attained in photon thick asymptotics. The largest transparency radii are reached instead in photon thin asymptotics.

Fig. 11 shows the energy-baryonic loading diagram, where the regions of validity of the asymptotics discussed above are indicated explicitly for typical parameters of GRBs. For all the relevant range of GRBs parameters 10^{48} erg $< E_0 < 10^{55}$ erg and 10^6 cm $< R_0 < 10^{12}$ cm all four asymptotics are present in the interval $10^{-10} < B < 10^{-1}$.

Using (18) we obtain for the electron-positron contribution to opacity

$$n_{\pm}/n = 2.5 \cdot 10^{-5} R_8^{3/4} B_2^{-1} E_{54}^{-1/4}, \quad (81)$$

after their decoupling, so it is clear that this contribution may be safely neglected for, say, $B > 10^{-4}$.

In photon thin case, expressing the peak arrival time (61) in units of total energy and baryonic loading, we find

$$t_p \simeq 1 E_{54}^{1/2} B_2^{5/2} s, \quad (82)$$

This expression gives an estimate for duration of photospheric emission in arrival time, and we conclude that typically this duration should be smaller than one second. Notice that t_p does not depend on R_0 and, consequently, on the light crossing time of the outflow. Currently time resolved spectra of GRBs with good statistics cannot resolve such small time scales, and therefore we expect that only time integrated spectra may be observed from GRBs which have their parameters corresponding to the photon thin case. Thus, starting from comoving thermal spectrum for the photospheric emission we obtain for the first time an observed spectrum which may be well described by the Band function with high energy power law index β being determined by the density profile of the outflow. We find this result quite remarkable. Notice that the idea of convolution over time has been introduced for GRBs by Blinnikov et al. (1999). Double convolution over EQTS and arrival time is also one of the key ideas in the fireshell model (Ruffini et al. 2003).

It is even more remarkable that GRBs appear to be the only objects in nature able to reach the photon thin asymptotics in their ultrarelativistic expansion. For thermally accelerated relativistic plasmas which are discussed in connec-

tion with their possible synthesis in ground based laboratories (e.g. Ruffini et al. (2010)) it is unreachable. In order to quantify what should be initial optical depth $\tau_0 = \sigma_T n_0 l$ in order to reach the photon thin asymptotics one may use (29) to get

$$\tau_0 \gg 4\Gamma^4 = 4 \times 10^8 B_2^{-4}. \quad (83)$$

GRBs clearly satisfy this constraint with the contribution of baryons only

$$\tau_0 = \frac{3\sigma_T B E_0}{4\pi m_p c^2 l^2} \simeq 10^{14} E_{54} B_2 R_8^{-2}. \quad (84)$$

which is increased even further by the presence of electron-positron pairs.

In contrast, in photon thick case the corresponding observed spectrum, as it is well known in the literature, is a black body with small deviations present at both low and high energy parts of the spectrum. It remains close to thermal also when variation of the Lorentz factor through the outflow is present (Daigne & Mochkovitch 2002).

When the outflow becomes transparent in the transition from photon thick to photon thin conditions, the observed spectrum will contain the Band component produced by the photon thin layer, with an almost black body coming from the photon thick part superimposed. As we already mentioned, in any outflow there is always a photon thin layer. So when the photon thick part becomes dominant, the spectrum is expected to be dominated by the black body component. This may be the reason why in most cases analysed by Ryde & Pe'er (2009) there are both power law and black body components: transparency occurs at the boundary between photon thin and photon thick conditions.

In Sec. 5.3 we give analytic expressions for the photon flux for the simple model of the portion of wind (17). With more complex density profile composed of presumably many shells the light curve is expected to be variable and arbitrarily complex. It is necessary to emphasize however, that the decaying part of the light curve is determined solely by the geometry of the limiting surfaces in photon thick (36) and photon thin (38) cases, respectively. So when the photon flux is observed with faster than t^{-3} decay it should be concluded that the emission does not come from the photosphere. The photospheric emission may be additionally identified by the spectral analysis. What we have shown here, though, is that the observed

spectrum may not necessarily be close to thermal, but in the photon thin case it may look very different.

7.2. Wind model

In the case of gradual energy release resulting in relativistic wind an additional parameter is present, that is the duration of energy release, which we parametrize as $\Delta t = \Delta t_1$ s. Instead of the total energy E_0 the luminosity $L = 10^{50} L_{50}$ erg/s will be used.

From formulae (15), (25), and (31) we obtain for the transparency radius

$$R_{tr} = \begin{cases} \frac{1}{T_{tr}} \left(\frac{LR_0^2}{4\pi c a} \right)^{1/4} = 8.1 \times 10^8 L_{50}^{1/4} R_8^{1/2} \text{ cm}, \\ L_{50} \ll 5.3 \times 10^{-15} B_{-2}^{-4} R_8^{-2}, \\ \left(\frac{\sigma L B R_0^2}{24\pi m_p c^3} \right)^{1/3} = 1.3 \times 10^{10} (L_{50} B_{-2} R_8^2)^{1/3} \text{ cm}, \\ 5.3 \times 10^{-15} B_{-2}^{-4} R_8^{-2} \ll L_{50} \ll 9.8 \times 10^{-2} B_{-2}^{-4} R_8, \\ \frac{\sigma L B^3}{8\pi m_p c^3} = 5.9 \times 10^{10} L_{50} B_{-2}^3 \text{ cm}, \\ 9.8 \times 10^{-2} B_{-2}^{-4} R_8 \ll L_{50} \ll 10^5 B_{-2}^{-5} \Delta t_1, \\ \left(\frac{\sigma L B \Delta t}{4\pi m_p c^2} \right)^{1/2} = 5.9 \times 10^{10} (L_{50} \Delta t_1 B_{-2})^{1/2} \text{ cm}, \\ L_{50} \gg 10^5 B_{-2}^{-5} \Delta t_1. \end{cases} \quad (85)$$

In Fig. 13 we show as function of the baryonic loading parameter the following quantities computed at the transparency radius: the Lorentz factor, the observed and comoving LOS temperatures, fraction of energy emitted from the photosphere to the total energy, for different duration of the wind with the total energy $E_0 = 10^{51}$ erg, and inner boundary radius $R_0 = 10^8$ cm. Wind duration ranges from 10 ms to 10 s. The corresponding wind luminosity varies from 10^{53} erg/s to 10^{50} erg/s. Fig. 14 shows the luminosity-baryonic loading diagram where the regions of validity of the asymptotics discussed above are indicated. Photon thin asymptotics is not common for the typical parameters of wind considered in the literature, but still can be relevant for energetic winds of short duration. Dependence of transparency parameters on the initial conditions of the wind is presented in Tab. 2.

All the discussion on the complexity of light curves for shell models is valid for wind models as well. Due to smaller range of applicability of photon thin asymptotics we expect that relativistic winds produce spectrum which is close to thermal one.

Generally speaking, for both shell and wind models with more complex number density, energy density and Lorentz factor distributions within the outflow various light curves and observed spectra of photospheric emission may be obtained,

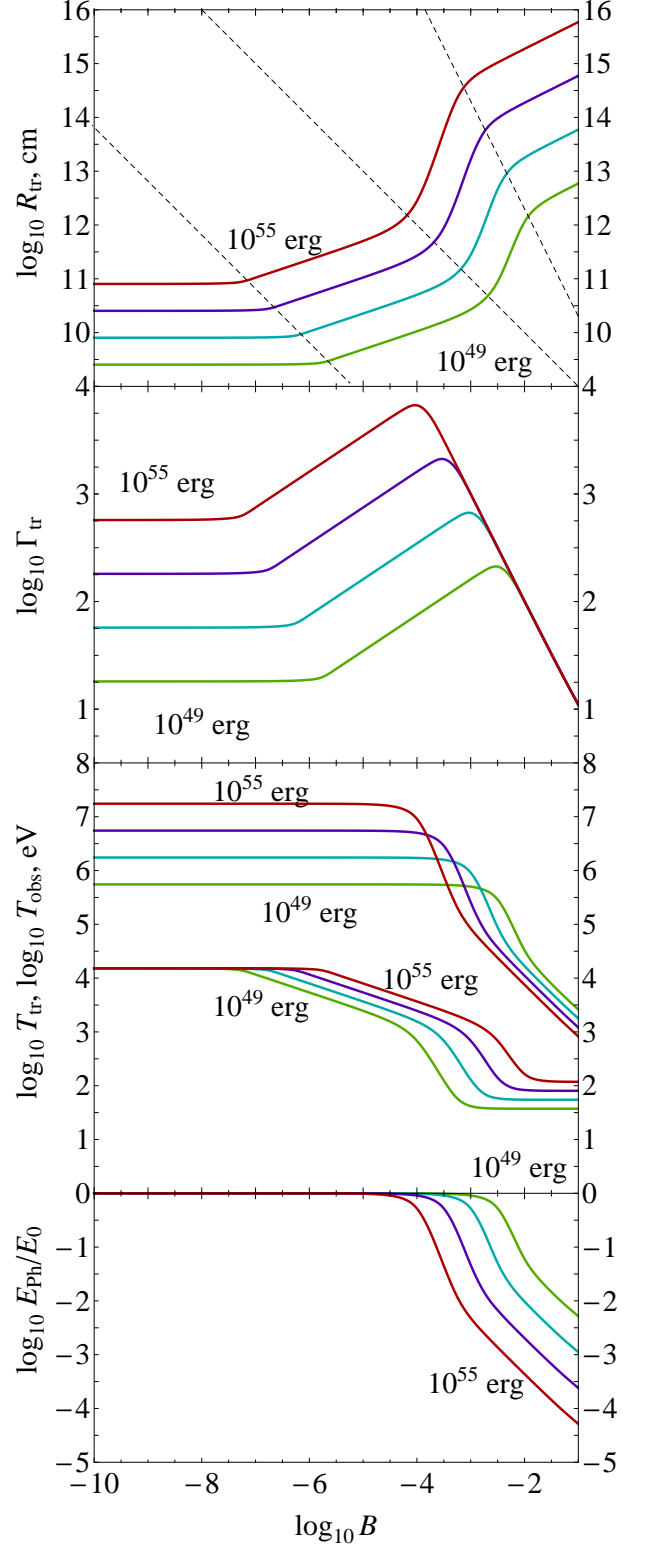


FIG. 12.— Transparency radius R_{tr} , Lorentz factor Γ_{tr} , observed T_{obs} and comoving T_{tr} temperatures, and ratio of the energy emitted to the total energy E_{ph}/E_0 at transparency radius as functions of baryonic loading B for shells with different total energy E_0 but the same width $l = R_0 = 10^8$ cm. All four regimes with different asymptotics are clearly visible and dashed lines corresponding to their domain of validity from Eq. (80) are shown. Curves are drawn for E_0 equal to 10^{49} erg (green), 10^{51} erg (blue), 10^{53} erg (violet), and 10^{55} erg (red).

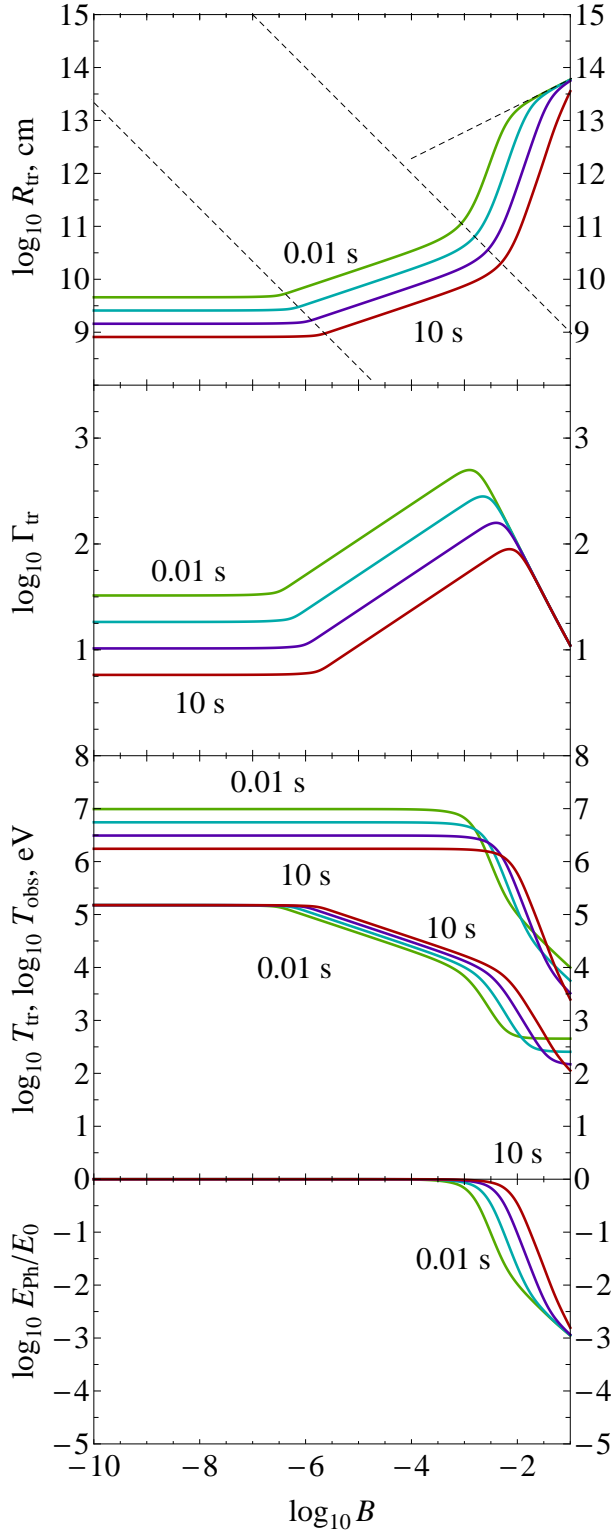


FIG. 13.— The same as in Fig. 12 for winds with different duration, but the same total energy $E_0 = 10^{51}$ erg and radius of origin $R_0 = 10^8$ cm. All four regimes with different asymptotics are clearly visible. Curves are drawn for Δt from to 10^{-2} s (green) to 10 s (red) in steps of one order of magnitude.

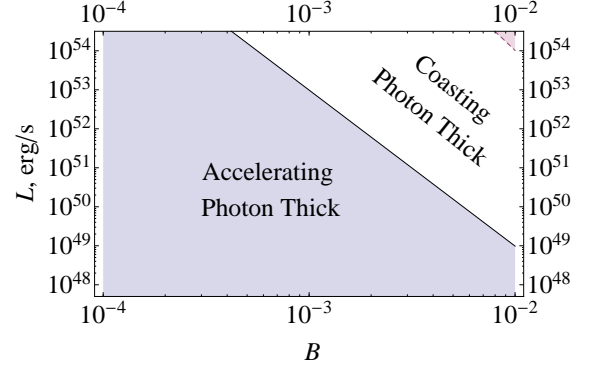


FIG. 14.— The luminosity-baryonic loading diagram showing the validity of the various asymptotic solutions for transparency radius of wind with duration $\Delta t = 0.1$ s. Notation is the same as on Fig. 11.

with the geometrical constraints discussed in previous sections. The theory developed in this paper may be used for the calculation of these observed quantities using the corresponding profiles obtained from e.g. hydrodynamic simulations. We plan to report on this study elsewhere (Ruffini et al. 2011).

8. CONCLUSIONS

In summary, in this paper we readdressed the issue of photospheric emission from spherically symmetric relativistic outflows. Two types of outflows are discussed: winds resulting from gradual energy release, and shells produced by instant energy release. We evaluated the optical depth and the corresponding photospheric radius for each type of the outflow. We demonstrated that there are two asymptotic solutions for a coasting shell, similarly to a coasting wind. In particular we showed that due to ultrarelativistic motion a geometrically thin shell may appear as thick for photons propagating inside it. For this reason we suggest to refer to any relativistic outflow as photon thick, when the photon spends enough time inside it to feel its density decreasing with time or radius. In the opposite case we refer to the outflow as photon thin.

We also studied geometry and dynamics of photospheres of relativistic outflows. As we are interested in appearance of the photosphere to a distant observer, we introduced the notion of photospheric equitemporal surface, the PhE. While in general the PhE is dynamically evolving, we showed that it is well approximated by a part of an ellipsoid in the case of the photon thin outflow. The photon thick PhE initially looks the same, due to the presence of photon thin layer in any outflow. Then it becomes concave and approaches asymptotically the photosphere of infinitely long wind.

Then, assuming that photons are trapped in the outflow with thermal and isotropic distribution for optical depth greater than one, and are release to freely stream when opacity decreases below one, we computed both photon flux and observed spectra of photon thick and photon thin outflows. Our adiabatic approximation corresponds to an assumption that the last scattering surface of photons is well defined. This assumption is shown to work in the photon thin case. As for photon thick case, our results for observed flux are shown to agree with other results in the literature, obtained with more accurate methods (Beloborodov 2011), see also (Pe'er & Ryde 2011).

We find that instantaneous spectra of both photon thick and photon thin outflows are close to the thermal one. This result is in agreement with the corresponding results in the litera-

ture for relativistic winds, since such winds with long enough duration must indeed be photon thick. However, the time integrated spectrum from photon thin outflows appears to be non thermal, due to strong temperature and luminosity evolution in arrival time. This spectrum may be described by the Band function (Band et al. 1993) with some specific low energy and high energy power law indices, and an exponential cutoff corresponding to the temperature in the source of energy release.

Our results are then applied to GRBs. We show in particular, that instantaneous spectra cannot be observed in the

case of photon thin outflows, and we predict therefore that typical observed spectrum originating from the photospheric emission should be the Band spectrum. Our analysis for simple density profile gives values for the low energy power law index $\alpha \simeq 0.5$ and the high-energy power law index $\beta = -4$, which are different from the typical values observed in GRBs. The low energy index is insensitive to both density and temperature profiles adopted. The high energy index strongly depends on the density profile, and it may vary from $-\infty$ to -1 .

REFERENCES

- Abramowicz, M. A., Novikov, I. D., & Paczynski, B. (1991). The appearance of highly relativistic, spherically symmetric stellar winds. *ApJ*, 369, 175–178.
- Aksenov, A. G., Ruffini, R., & Vereshchagin, G. V. (2007). Thermalization of Nonequilibrium Electron-Positron-Photon Plasmas. *Phys. Rev. Lett.*, 99(12), 125003–+.
- Aksenov, A. G., Ruffini, R., & Vereshchagin, G. V. (2009). Thermalization of the mildly relativistic plasma. *Phys. Rev. D*, 79(4), 043008.
- Aksenov, A. G., Ruffini, R., & Vereshchagin, G. V. (2010). Pair plasma relaxation time scales. *Phys. Rev. E*, 81, 046401.
- Band, D., Matteson, J., Ford, L., Schaefler, B., Palmer, D., Teegarden, B., Cline, T., Briggs, M., Paciesas, W., Pendleton, G., Fishman, G., Kouveliotou, C., Meegan, C., Wilson, R., & LeStrade, P. (1993). BATSE observations of gamma-ray burst spectra. I - Spectral diversity. *ApJ*, 413, 281–292.
- Beloborodov, A. M. (2011). Radiative Transfer in Ultrarelativistic Outflows. *ApJ*, 737, 68–+.
- Bianco, C. L., Ruffini, R., & Xue, S. (2001). The elementary spike produced by a pure e^+e^- pair-electromagnetic pulse from a Black Hole: The PEM Pulse. *A&A*, 368, 377–390.
- Blinnikov, S. I., Kozyreva, A. V., & Panchenko, I. E. (1999). Gamma-ray bursts: When does a blackbody spectrum look non-thermal? *Astronomy Reports*, 43, 739–747.
- Chiang, J. & Dermer, C. D. (1999). Synchrotron and Synchrotron Self-Compton Emission and the Blast-Wave Model of Gamma-Ray Bursts. *ApJ*, 512, 699–710.
- Couderc, P. (1939). Les aureoles lumineuses des Novaelig. *Annales d'Astrophysique*, 2, 271–+.
- Daigne, F. & Mochkovitch, R. (2002). The expected thermal precursors of gamma-ray bursts in the internal shock model. *MNRAS*, 336, 1271–1280.
- Fenimore, E. E., Madras, C. D., & Nayakshin, S. (1996). Expanding Relativistic Shells and Gamma-Ray Burst Temporal Structure. *ApJ*, 473, 998–+.
- Genet, F. & Granot, J. (2009). Realistic analytic model for the prompt and high-latitude emission in GRBs. *MNRAS*, 399, 1328–1346.
- Goodman, J. (1986). Are gamma-ray bursts optically thick? *ApJ*, 308, L47–L50.
- Granot, J., Piran, T., & Sari, R. (1999a). Images and Spectra from the Interior of a Relativistic Fireball. *ApJ*, 513, 679–689.
- Granot, J., Piran, T., & Sari, R. (1999b). Images, light curves and spectra of GRB afterglow. *A&AS*, 138, 541–542.
- Grimmsrud, O. M. & Wasserman, I. (1998). Non-equilibrium effects in steady relativistic $e^+ + e^-$ -gamma winds. *MNRAS*, 300, 1158–1180.
- Li, C. & Sari, R. (2008). Analytical Solutions for Expanding Fireballs. *ApJ*, 677, 425–431.
- Lyutikov, M. (2006). The electromagnetic model of gamma-ray bursts. *New Journal of Physics*, 8, 119–+.
- Maraschi, L. (2003). Jets at different scales. In S. Collin, F. Combes, & I. Shlosman (Eds.), *Active Galactic Nuclei: From Central Engine to Host Galaxy*, volume 290 of *Astronomical Society of the Pacific Conference Series* (pp. 275–+).
- Mészáros, P., Laguna, P., & Rees, M. J. (1993). Gasdynamics of relativistically expanding gamma-ray burst sources - Kinematics, energetics, magnetic fields, and efficiency. *ApJ*, 415, 181–190.
- Mészáros, P., Ramirez-Ruiz, E., Rees, M. J., & Zhang, B. (2002). X-Ray-rich Gamma-Ray Bursts, Photospheres, and Variability. *ApJ*, 578, 812–817.
- Mészáros, P. & Rees, M. J. (2000). Steep Slopes and Preferred Breaks in Gamma-Ray Burst Spectra: The Role of Photospheres and Comptonization. *ApJ*, 530, 292–298.
- Nakar, E., Piran, T., & Sari, R. (2005). Pure and Loaded Fireballs in Soft Gamma-Ray Repeater Giant Flares. *ApJ*, 635, 516–521.
- Paczynski, B. (1986). Gamma-ray bursters at cosmological distances. *ApJ*, 308, L43–L46.
- Paczynski, B. (1990). Super-Eddington winds from neutron stars. *ApJ*, 363, 218–226.
- Pauli, W. (1958). *Theory of relativity*. Dover books on relativity and related areas. Pergamon Press.
- Pe'er, A. (2008). Temporal Evolution of Thermal Emission from Relativistically Expanding Plasma. *ApJ*, 682, 463–473.
- Pe'er, A. & Ryde, F. (2011). A Theory of Multicolor Blackbody Emission from Relativistically Expanding Plasmas. *ApJ*, 732, 49–+.
- Pe'er, A., Ryde, F., Wijers, R. A. M. J., Mészáros, P., & Rees, M. J. (2007). A New Method of Determining the Initial Size and Lorentz Factor of Gamma-Ray Burst Fireballs Using a Thermal Emission Component. *ApJ*, 664, L1–L4.
- Piran, T. (1999). Gamma-ray bursts and the fireball model. *Phys. Rep.*, 314, 575–667.
- Piran, T. (2004). The physics of gamma-ray bursts. *Reviews of Modern Physics*, 76, 1143–1210.
- Piran, T., Shemi, A., & Narayan, R. (1993). Hydrodynamics of Relativistic Fireballs. *MNRAS*, 263, 861–867.
- Rees, M. J. (1966). Appearance of Relativistically Expanding Radio Sources. *Nature*, 211, 468–470.
- Rees, M. J. (1967). Studies in radio source structure-I. A relativistically expanding model for variable quasi-stellar radio sources. *MNRAS*, 135, 345–+.
- Ruffini, R., Aksenov, A., Bernardini, M. G., Bianco, C. L., Caito, L., Dainotti, M. G., de Barros, G., Guida, R., Vereshchagin, G., & Xue, S. (2009). The canonical Gamma-Ray Bursts: long, “fake”-“disguised” and “genuine” short bursts. In G. Giobbi, A. Tornambe, G. Raimondo, M. Limongi, L. A. Antonelli, N. Menci, & E. Brocato (Ed.), *American Institute of Physics Conference Series*, volume 1111 of *American Institute of Physics Conference Series* (pp. 325–332).
- Ruffini, R., Bianco, C. L., Chardonnet, P., Frascchetti, F., Vitagliano, L., & Xue, S. (2003). New perspectives in physics and astrophysics from the theoretical understanding of Gamma-Ray Bursts. In *AIP Conf. Proc. 668: Cosmology and Gravitation* (pp. 16–107).
- Ruffini, R., Bianco, C. L., Chardonnet, P., Frascchetti, F., & Xue, S. (2002). On the Structures in the Afterglow Peak Emission of Gamma-Ray Bursts. *ApJ*, 581, L19–L22.
- Ruffini, R., Salmonson, J. D., Wilson, J. R., & Xue, S.-S. (2000). On the pair-electromagnetic pulse from an electromagnetic black hole surrounded by a baryonic remnant. *A&A*, 359, 855–864.
- Ruffini, R., Siutsou, A., & Vereshchagin, G. (2011). in preparation.
- Ruffini, R., Vereshchagin, G., & Xue, S.-S. (2010). Electron-positron pairs in physics and astrophysics. *Physics Reports*, 487, 1–140.
- Rybicki, G. B. & Lightman, A. P. (1979). *Radiative processes in astrophysics*.
- Ryde, F. & Pe'er, A. (2009). Quasi-blackbody Component and Radiative Efficiency of the Prompt Emission of Gamma-ray Bursts. *ApJ*, 702, 1211–1229.
- Ryde, F., Pe'er, A., Nymark, T., Axelsson, M., Moretti, E., Lundman, C., Batelino, M., Bissaldi, E., Chiang, J., Jackson, M. S., Larsson, S., Longo, F., McGlynn, S., & Omodei, N. (2011). Observational evidence of dissipative photospheres in gamma-ray bursts. *ArXiv e-prints*.
- Shemi, A. & Piran, T. (1990). The appearance of cosmic fireballs. *ApJ*, 365, L55–L58.
- Toma, K., Wu, X.-F., & Mészáros, P. (2011). Photosphere-internal shock model of gamma-ray bursts: case studies of Fermi/LAT bursts. *MNRAS*, 415, 1663–1680.
- Woods, E. & Loeb, A. (1999). Constraints on Off-Axis X-Ray Emission from Beamed Gamma-Ray Bursts. *ApJ*, 523, 187–191.

In this Appendix we consider the optical depth for photons emitted from different layers of an ultrarelativistically expanding shell in the coasting phase. The density of the shell in the laboratory frame is

$$n(r, t=0)\Gamma = \begin{cases} n_0, & L-l \leq r \leq L, \\ 0, & r > L \text{ or } r < L-l. \end{cases} \quad (86)$$

Continuity equation gives

$$n(r, t)\Gamma = \begin{cases} n_0 \frac{(r-vt)^2}{r^2}, & L-l+vt \leq r \leq L+vt, \\ 0, & r > L+vt \text{ or } r < L-l+vt. \end{cases} \quad (87)$$

The trajectory of the photon emitted in the radial direction from a radius R at time T is $r(t) = R + c(t - T)$. The radius at which the photon leaves the shell in the ultrarelativistic approximation is

$$R + \Delta R \simeq R + 2\Gamma^2 \xi,$$

where $\xi = L + vT - R$ denotes the distance from the radius of emission to the outer boundary of the shell. From (8) the optical depth for such a photon is

$$\begin{aligned} \tau(R, T) &= \int_R^{R+\Delta R} \sigma n(r, T + \frac{r-R}{c}) \Gamma (1-\beta) dr \simeq \\ &\simeq \frac{\sigma n_0 R}{8\Gamma^6} \left[\frac{2\Gamma^2 \xi}{R} + 2 \left(\frac{2\Gamma^2(R-cT)}{R} \right) \log \left(1 + \frac{2\Gamma^2 \xi}{R} \right) + \left(\frac{2\Gamma^2(R-cT)}{R} \right)^2 \left(1 - \frac{1}{1 + \frac{2\Gamma^2 \xi}{R}} \right) \right]. \end{aligned} \quad (88)$$

We are interested in the time evolution of the optical depth for photons emitted in the radial direction from a given layer of the shell. Then the radius of emission and time of emission are connected by the equation of motion of the layer $R = L - \xi + vT$. The optical depth for the chosen layer is

$$\tau(R) = \frac{\sigma n_0 R}{8\Gamma^6} \left[\frac{2\Gamma^2 \xi}{R} + 2 \left(\frac{2\Gamma^2 \lambda}{R} - 1 \right) \log \left(1 + \frac{2\Gamma^2 \xi}{R} \right) + \left(\frac{2\Gamma^2 \lambda}{R} - 1 \right)^2 \left(1 - \frac{1}{1 + \frac{2\Gamma^2 \xi}{R}} \right) \right], \quad (89)$$

where $\lambda = L - \xi$.

This expression has three asymptotic limits

$$\tau = \begin{cases} \sigma n_0 \frac{\lambda^2 \xi}{R^2}, & \frac{2\Gamma^2 \xi}{R} \ll 1, \\ \sigma n_0 \frac{\lambda^2}{2\Gamma^2 R}, & 1 \ll \frac{2\Gamma^2 \xi}{R} \ll \left(\frac{2\Gamma^2 \lambda}{R} - 1 \right)^2, \\ \sigma n_0 \frac{\xi}{4\Gamma^4}, & 1 \ll \left(\frac{2\Gamma^2 \lambda}{R} - 1 \right)^2 \ll \frac{2\Gamma^2 \xi}{R}, \end{cases} \quad (90)$$

but only the first two are of interest for $l \ll L$.

Using (19) we finally have

$$\tau = \begin{cases} \frac{\sigma E_0 B^3}{8\pi m_p c^2} \frac{1}{Rl}, & R \ll \frac{\xi}{1-\beta}, \\ \frac{\sigma E_0 B}{4\pi m_p c^2} \frac{\xi}{lR^2}, & R \gg \frac{\xi}{1-\beta}. \end{cases} \quad (91)$$

Both lines in (91) coincide with (29) for $\xi = l$, namely when the photon is emitted from the internal boundary of an expanding outflow.

APPENDIX B

We consider coasting photon thin outflow with arbitrary laboratory density profile (6). Blooming velocity (72) can be obtained from the arrival time t_a for the photon thin outflow

$$t_a \simeq \frac{R_e}{\beta c} (1 - \beta \mu), \quad (92)$$

and the optical depth of the outflow for its differential layer $\xi = \text{const}$ within relativistic beaming angle $\mu = \beta$

$$\tau \simeq \frac{\sigma n_0 R_0^2}{R_e^2} \frac{1 - \beta \mu}{\mu - \beta} g(\xi) = \frac{\sigma n_0 R_0^2}{(\beta c t_a)^2} \frac{(1 - \beta \mu)^3}{\mu - \beta} g(\xi), \quad (93)$$

where

$$g(\xi) = \int_0^\xi f(\xi) d\xi. \quad (94)$$

The result is

$$v_b = \frac{d\xi}{dt_a} \simeq \frac{2g(\xi)}{t_a f(\xi)} = \frac{1}{f(\xi)} \frac{2\beta^2 c^2 t_a}{\sigma n_0 R_0^2} \frac{\mu - \beta}{(1 - \beta\mu)^3}, \quad (95)$$

where corresponding ξ should be found by equating (93) to unity. Since the form of PhE and its temperature distribution for photon thin outflow does not depend on the depth ξ and on the shape of density profile $f(\xi)$, the difference in observed spectra comes from the variation in blooming velocities only, by changing relative intensity of thermal spectra at different t_a . Therefore the high-energy part of time-integrated spectrum of photon thin outflow strongly depends on its density profile $f(\xi)$.

In order to illustrate this dependence consider the following power law density profile

$$f(\xi) = (\xi/l)^\delta, \quad (96)$$

where $\delta > -1$ is a constant. For $g(\xi)$ we obtain

$$g(\xi) = \frac{l}{\delta+1} (\xi/l)^{\delta+1} \quad (97)$$

and the blooming velocity is

$$v_b = 2t_a^{\frac{1-\delta}{1+\delta}} \left[\frac{\beta^2 c^2}{\sigma n_0 R_0^2} \frac{\mu - \beta}{(1 - \beta\mu)^3} \left(\frac{l}{1+\delta} \right)^\delta \right]^{\frac{1}{1+\delta}}. \quad (98)$$

The main contribution to time-integrated spectrum F_ν comes from the maximum of instantaneous spectrum which is a function of arrival time. Its position is $kT_{LOS}(t_a) \simeq h\nu$ and its value is

$$F_\nu(t_a) \propto \frac{\nu^3}{\exp\left(\frac{h\nu}{kT}\right)} \propto T_{LOS}(t_a)^3 \propto t_a^{-2}, \quad (99)$$

where last proportionality is the consequence of (75) and (92). This approximation will be valid near $t_a \sim \frac{R_0}{2\Gamma^2 c} \left(\frac{kT_0}{h\nu} \right)^{3/2}$ and using (73) we arrive to the following final expression for time-integrated flux

$$F_\nu \propto \int_{a/\nu^{3/2}}^{b/\nu^{3/2}} dt_a t_a^{\frac{1-\delta}{1+\delta}} \propto \nu^{-\frac{3}{1+\delta}}, \quad (100)$$

where a and b are some constants which are selected in such a way that total flux is equal to the thermal one. This approximation is valid for photon energies $h\nu$ between initial thermal energy kT_0 and minimal observed thermal energy along the line of sight $kT_{LOS,min} = kT_0 (R_0\Gamma/R_{tr})^{2/3}$.